Controls on the ocean response to idealized Antarctic meltwater input

Rory Basinski-Ferris[a,b] , Laure Zanna[a] , Ian Eisenman[b]

[a] *Courant Institute of Mathematical Sciences, New York University, New York, NY, USA*
[b] *Scripps Institution of Oceanography, University of California San Diego, La Jolla, CA, USA*

ABSTRACT: Antarctic meltwater is expected to increase throughout the coming centuries and impact sea level, ocean circulation, and the coupled climate evolution. This motivates interest in understanding the ocean response to Antarctic freshwater injection, including potential sources of uncertainty. In this study, we use idealized single-basin ocean simulations with meltwater input to examine the dependence of ocean transport and the timescales of the adjustment of regional sea level patterns on: (a) the model resolution and parameter values such as the mesoscale eddy Gent-McWilliams parameterization and vertical diffusivity, thereby partially addressing structural and parametric uncertainty; and (b) the depth of meltwater forcing, which must be prescribed both in our experiments and in most comprehensive climate model simulations, due to a lack of dynamic coupling with an ice sheet model. We find distinct sea level adjustment timescales and changes in the upper and abyssal cells depending on the depth of input, including a near total shutdown of the abyssal cell which only occurs with meltwater injection at the surface. We additionally demonstrate strong connections between the adjustment of key variables, such as regional sea level, and the background stratification in the control simulation, which depends on the model resolution and parameter values. This indicates that the ocean state and physics substantially influence the dynamic ocean response to ice shelf meltwater, in addition to uncertainty in how ocean models interact with fluxes from ice sheets.

SIGNIFICANCE STATEMENT: The amount of meltwater that Antarctica releases into the ocean is expected to increase in the future. This study looks at uncertainties in how the ocean responds to Antarctic meltwater using an idealized single-basin ocean model. We show that the ocean model resolution and parameter values, as well as the depth of meltwater injection, affect the simulated ocean response. These results have implications for projections of ocean circulation and sea level changes.

1. Introduction

Antarctica has been losing mass over recent decades (e.g., Otosaka et al. 2023), with projections indicating continued mass loss during the coming centuries (e.g., Oppenheimer et al. 2019). This meltwater input from the Antarctic ice sheet raises sea level, with an inhomogeneous pattern determined by changes in gravitation, rotation, and solid-earth deformation (e.g., Farrell and Clark 1976; Kopp et al. 2010; Mitrovica et al. 2018) and changes in ocean dynamic processes (e.g., Stammer 2008; Lorbacher et al. 2012; Kopp et al. 2010; Schmidt et al. 2023). The introduction of Antarctic meltwater also affects the ocean state more broadly and has been demonstrated to change the large-scale ocean circulation including the abyssal cell (e.g., Lago and England 2019; Li et al. 2023a; Moon et al. 2025), change the ocean stratification, and lead to Southern Ocean surface cooling and subsurface warming (e.g., Bronselaer et al. 2018; Schmidt et al. 2023; Li et al. 2023b), amongst other impacts. Modulated by these effects on the ocean state, meltwater introduction is expected to additionally change the coupled climate response to anthropogenic forcing, including standard metrics such as the global mean temperature change (e.g., Bronselaer et al. 2018; Sadai et al. 2020; Li et al. 2023b), through influencing both ocean heat uptake and radiative feedbacks via the pattern effect (Dong et al. 2022). Thus, understanding the sensitivities of the modeled ocean dynamic response to Antarctic meltwater input is key for a wide range of climate change observables.

Simulated features of the ocean circulation, including large-scale systems such as the meridional overturning circulation and Antarctic Circumpolar Current, are sensitive to the grid resolution (e.g., Roberts et al. 2020; Marques et al. 2022) and choice of parameter values including vertical diffusivity (e.g., Mignot et al. 2006) and eddy diffusivities (e.g., Marshall et al. 2017; Saenko et al. 2018). This sensitivity affects both the control state and the response of the ocean to forcing (e.g., changes in the atmospheric CO_2 concentration) including projected changes in transport, heat uptake, and dynamic sea level (e.g., Saenko et al. 2018; Huber and Zanna 2017; Todd et al. 2020; Wickramage et al. 2023). While there have been explorations of these sensitivities for the atmosphere-ocean coupled system forced by anthropogenic emissions, they are yet to be explored when including interactions with ice sheets. Similar to the response to atmospheric fluxes, the impact of meltwater fluxes on the ocean state may also be expected to be sensitive to resolution and model parameter values, due to anticipated dependencies on the represented stratification and circulation (Swart

Corresponding author: Rory Basinski-Ferris, rbasinskiferris@ucsd.edu

et al. 2023). This sensitivity will introduce uncertainty in projections of the response to Antarctic meltwater stemming from the ocean model set-up alone, which has not previously been systematically explored.

The introduction of meltwater into the model ocean is associated with its own uncertainty, partially because most current coupled climate models, including those in phases 5 and 6 of the Coupled Model Intercomparison Project (CMIP), have fixed ice sheets which do not interact with the ocean (Taylor et al. 2012; Eyring et al. 2016). Thus, the basal melt of ice shelves, which is a dominant source of mass loss (e.g., Pritchard et al. 2012; Rignot et al. 2013; Depoorter et al. 2013), is not dynamically represented. Due to this lack of coupling, choices must be made regarding the magnitude and spatiotemporal distribution of prescribed meltwater input, with current community efforts aimed at investigating the sensitivity to these choices (Swart et al. 2023). For example, one such choice that needs to be made is the depth of meltwater prescription, which has typically been chosen to be at the ocean surface (e.g., Stammer 2008; Lorbacher et al. 2012; Kopp et al. 2010; Bronselaer et al. 2018; Golledge et al. 2019; Moorman et al. 2020; Li et al. 2023b; Schmidt et al. 2023; Park et al. 2023), whereas observational evidence implies that much of the flux occurs considerably below the surface (Kim et al. 2016; Garabato et al. 2017), potentially dependent on the local stratification (Arnscheidt et al. 2021). Eisenman et al. (2024) and Basinski-Ferris et al. (2025) recently demonstrated that the depth of the meltwater flux has a substantial impact on the ocean dynamical response and sea level.

Here, we investigate how the ocean response to meltwater depends on modelling choices, including the ocean model parameter values. In particular, we investigate the impact of different ocean states on the global adjustment of the ocean to both surface and subsurface idealized meltwater input to highlight physical dependencies of the response. We use idealized meltwater input and a simplified model set-up to systematically explore a wide range of ocean model parameter perturbations and assess their impact on the ocean's response. This follows previous literature on perturbed parameter ensembles where parameters are varied through a range of values to sample model uncertainty (e.g., Leutbecher et al. 2017; Zanna et al. 2019; Eidhammer et al. 2024). For each of the resultant ocean states, we examine the adjustment of meltwater input at both the surface and at depth in order to capture uncertainty in how the meltwater is prescribed into the ocean.

2. Methods

a. Model configuration and spin up

We use the MITgcm ocean model (Marshall et al. 1997) in an idealized single-basin domain which spans from -62° to 62° in latitude and 0° to 42° in longitude. The basin has continental shelves which linearly slope down to the full depth of 5500m, and includes a re-entrant channel with a ridge at 2750m depth (see Figure 1a). This set-up is similar to Munday et al. (2013), but with a wider basin and continental shelves. Our single-basin geometry allows for a large number of perturbed parameter runs at lower computational cost than realistic geometry and resembles the domain used in many previous studies (e.g., Jansen et al. 2018; Jones et al. 2011; Marques et al. 2022).

We utilize models with both 1° and $\frac{1}{4}^\circ$ horizontal resolution. For both, we use no-slip boundary conditions, an implicit nonlinear free surface, and a convective adjustment scheme which applies a high vertical diffusivity (1 m^2/s) to mix unstable density profiles. We employ a nonlinear equation of state which is a modified UNESCO formula by Jackett and Mcdougall (1995). The vertical diffusivity (κ_v) is a function of depth (Bryan and Lewis 1979), with the default profile shown in orange in Figure 1d. In the 1° set-up, we use Laplacian horizontal viscosity, whereas in the $\frac{1}{4}^\circ$ set-up we use Smagorinsky horizontal biharmonic viscosity. In the 1° runs, we use the Gent-McWilliams (GM) parameterization (Gent and McWilliams 1990) with a constant isopycnal thickness diffusivity set to 1000 m^2s^{-1} by default and the Redi isopycnal tracer diffusivity (Redi 1982) set equal to the GM parameter (Figure 1b); throughout the text we refer to this as the $\kappa_{GM/Redi}$ parameter. We use no GM or Redi parameterization in the $\frac{1}{4}^\circ$ runs.

We begin with a long spin-up run in 1° resolution with the default vertical diffusivity profile and $\kappa_{GM/Redi}$ parameter value. The spin-up run imposes zonal wind in the southern part of the domain shown in Figure 1e and relaxes the sea surface temperature (SST) and sea surface salinity (SSS) to specified profiles (see Figure 1f/g). The relaxation timescales are set to 10 days and 30 days for SST and SSS, respectively. The 1° spin-up run is performed for 7540 years until there is equilibration of the deep ocean (see supplementary text S1 in Eisenman et al. (2024)).

To generate different ocean states, we initialize simulations starting from the default spin-up run, perturb the parameter values or resolution, and re-equilibrate the ocean with the restoring boundary conditions. In total, we create 18 versions of the model including one version at $\frac{1}{4}^\circ$ resolution and 17 versions at 1° resolution with different $\kappa_{GM/Redi}$ parameter values and vertical

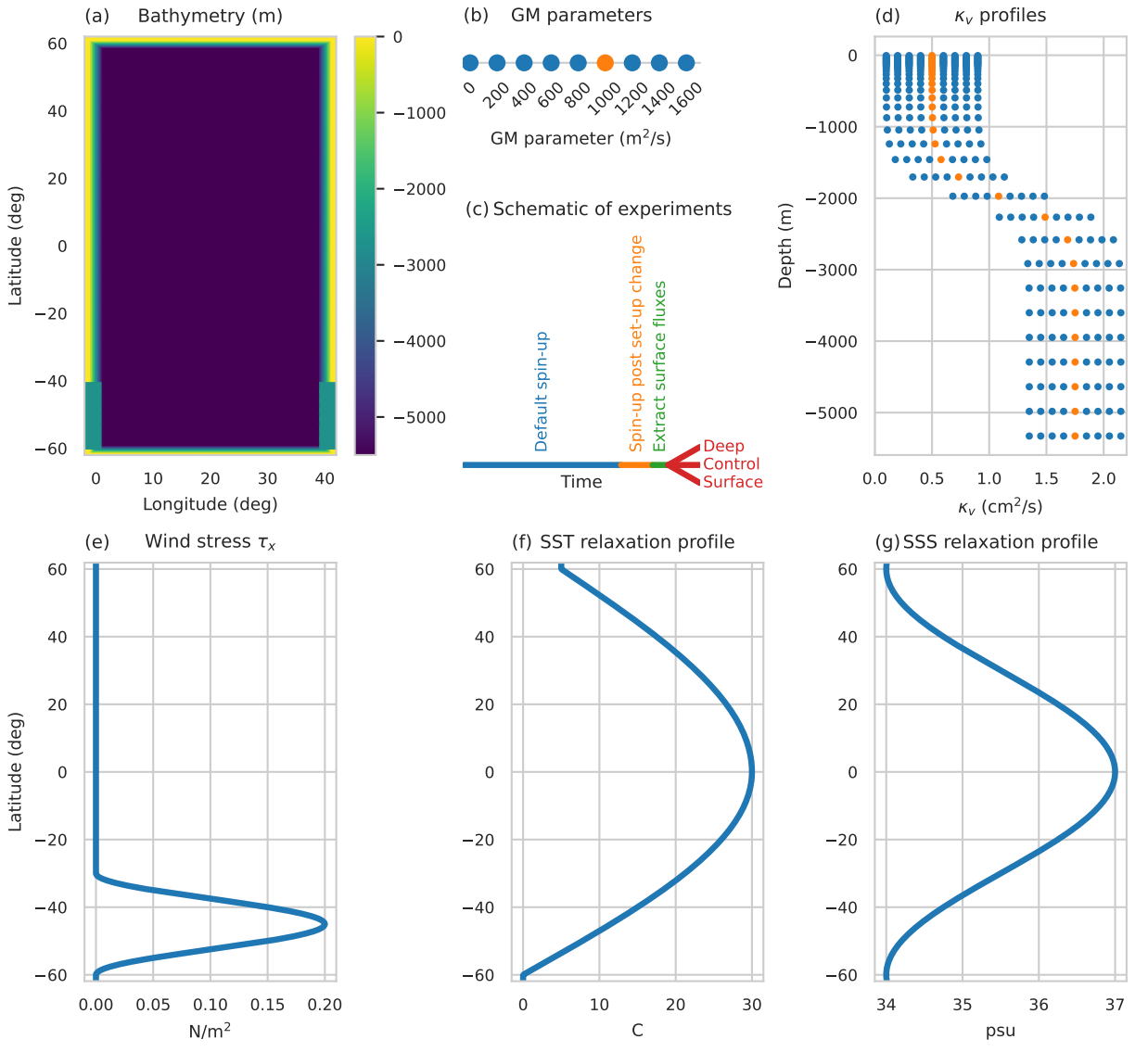

FIG. 1. Numerical model set-up. (a): The single basin bathymetry, identical to Eisenman et al. (2024), with linearly sloping continental shelves and a re-entrant channel with a ridge. (b): The values of the $\kappa_{GM/Redi}$ parameter in the simulations. (c) Schematic of experiments as described in text. Note that partway through the spin-up runs (shown in blue and orange), we switched from a linear free surface to a non-linear free surface, because the latter, which is less commonly used, perfectly conserves tracers. For the $\frac{1}{4}^\circ$ run, this switch was done at year 3414 (of the total additional 5726 year spin-up), while for the 1° runs, this was performed at the time of branching. (d) The different vertical diffusivity profiles considered. For both the GM parameter and the vertical diffusivity, unless the parameter is specified in text to be changed, the default values highlighted in orange are used in the coarse simulation. (e): The zonal wind stress profile, primarily applied in the Southern Ocean region. (f)/(g): The sea surface temperature (SST) and sea surface salinity (SSS) relaxation profiles utilized in the spin-up runs.

diffusivity profiles. For the 1° runs, we branch from the end of the 7540 year run and vary either $\kappa_{GM/Redi}$ (Figure 1b) or vertical diffusivity (Figure 1d), while holding the other at the default value. For each change from the default version of the model, we continue a spin-up run until equilibration after introducing the parameter change, with additional spin-up needed for between 200 and 1309 years; smaller parameter changes required less additional spin-up, while larger parameter changes needed more to achieve equilibration. The $\frac{1}{4}^\circ$ spin-up run was branched 600 years into the default 1° spin-up run, with an additional runtime to equilibration of 5726 years after the branching.

Parameter choices sampled in the different versions of the 1° model are similar to those in Huber and Zanna (2017) and Newsom et al. (2023), who chose parameter values consistent with CMIP5 to sample parametric uncertainty. These parameter choices are consistent with our aim of capturing a wide range of reasonable ocean states through which to understand dependencies of the ocean response to meltwater. We note that the parameters do not aim to fully capture parameter uncertainty across observations or newer state-of-the-art coupled model ensembles. For example, a common assumption, which we follow, is that different Bryan-Lewis profiles of vertical diffusivity have the same functional form and are only shifted by a constant at every depth (e.g., Ehlert et al. 2017; MacDougall et al. 2017; Huber and Zanna 2017; Newsom et al. 2023). This results in sampling less uncertainty in the deep ocean and oversampling in the upper ocean compared to the newest observational estimates (e.g., Oka 2025). Similarly, we vary the GM parameter but assume it is spatially constant, while the modeling community tends to favor a spatially varying parameter in some recent studies (Loose et al. 2023).

b. Surface flux boundary conditions

We aim to isolate and focus on the range of ocean dynamic responses to meltwater perturbations, and thus to examine the responses without damping from the surface boundary restoring (the idealized atmosphere). After the spin-up runs, for each model set-up, we prescribe surface fluxes rather than restoring boundary conditions following the protocol design of Zika et al. (2018) and Todd et al. (2020) and as also used in Eisenman et al. (2024).

For each run, we identify a 25-year period from the end of the spin-up run with near 0 global and temporal mean heat and salt fluxes; in practice, across all 18 model set-ups, the surface fluxes chosen from the end of the spin-up runs would result in volume mean drift of less than 4.0×10^{-5} K/year and 9.8×10^{-6} g/kg/year, which are the same orders of magnitude as in Eisenman et al. (2024). We perform a temporal mean over the identified period to generate a time-constant map of surface heat and (virtual) salt fluxes. This approach is in contrast to previous studies that extracted fluxes from the spin-up run with high temporal frequency (e.g., 6-hourly or daily) and then imposed them as a repeating cycle onto the ocean (e.g., Todd et al. 2020). In the case of previous literature, coarse resolution models were used, whereas in this work we include a $\frac{1}{4}^\circ$ eddy-permitting run, meaning that fluxes at high temporal resolution may be associated with transient eddies in the spin-up run. The temporal averaging approach avoids imposing fluxes with transient eddies from a spin-up run that are not associated with eddies in the flux-forced run. A trade-off of this approach is that imposing a climatology will likely impact the ocean response compared to high frequency fluxes (see Luongo et al. 2024, for an analysis of such issues in the case of wind forcing). This strategy is repeated for all runs, including the 1° runs, for consistency. For the eddy-permitting resolution ($\frac{1}{4}^\circ$) simulation, we generate an ensemble of 6 members to sample internal variability associated with the presence of eddies, each with its own fluxes found from non-overlapping 25-year periods near the end of the spin-up run. In all flux-forced simulations, we continue to use the same wind profile as in the restoring boundary runs (Figure 1e).

c. Meltwater injection

For each parameter set-up, we initiate three runs which all use the constant surface fluxes as outlined in Section 2b. These runs are (a) control with no meltwater input; (b) surface meltwater input; and (c) deep meltwater input. For both perturbation experiments, we add fluid into the ocean uniformly at the southernmost ocean cell (just north of the continental shelf). The surface meltwater experiment uses volume input at all longitudes in the top grid cell in z-space (between 0 and 10m depth), while in the deep meltwater experiment, we input water in the grid cell located around 1000m (between 954 and 1137m depth). The meltwater input is performed using the "AddMass" option in MITgcm, which inputs a real, rather than virtual, water flux (i.e., it changes the ocean volume). We input the water at 0°C and 0 psu.

The meltwater input is prescribed as a constant 0.1 Sv spread over all longitudes of the basin. This choice of input is large given the ice sheet mass balance in the current climate, but useful for comparison to previous literature (e.g., Bronselaer et al. 2018; Lago and England 2019; Bronselaer et al. 2020; Beadling et al. 2022; Eisenman et al. 2024) and to proposed Tier 1 experiments in Swart et al. (2023).

d. Metrics

In this paper, we focus on a few metrics to quantify the change in ocean states initiated by parameter value and resolution changes, as well as the response of the ocean to meltwater.

We use the meridional overturning streamfunction as a metric for the large scale circulation, ψ, which we compute in density coordinates and then remap to z-coordinates. In particular, we compute the following integral in potential density coordinates σ referenced to the surface (i.e., $\sigma = \sigma_0$):

$$\psi(y,\sigma,t) = \int_{\sigma_{\min}}^{\sigma}\int_{x_w}^{x_e} v(x,y,\sigma',t)\,dx\,d\sigma', \qquad (1)$$

with yearly averaged data and $\sigma_{\min}$ equal to the minimum potential density. Here, x_e and x_w are the locations of the eastern and western edges of the basin, respectively. We project ψ back to depth space using the yearly averaged depth (in z) of each isopycnal σ; thus, we remap $\psi(y,\sigma,t) \rightarrow \psi(y,z,t)$. In practice, Equation (1) is calculated using the "layers" package in MITgcm, where $v(x,y,\sigma,t)$ includes both the resolved and the bolus velocity from the GM parametrization (if utilized). The strength of the upper cell meridional overturning circulation (MOC) is computed as the maximum of ψ north of 20°N and below 300 meters depth, and the strength of the abyssal cell is the maximum of $|\psi|$ below 2000 meters (at any latitude, and thus typically set in the Southern Ocean). Note that values are sensitive to the coordinate used for streamfunction calculation – for example, if we had calculated the streamfunction in depth coordinates rather than potential density coordinates, the abyssal cell would be weaker due to cancellation from the Deacon cell (Döös and Webb 1994).

In the meltwater perturbation runs, we examine dynamic sea level which is defined at any point (or area) as the anomaly of the model free surface (η) from the global mean. We focus on the Northern Hemisphere dynamic sea level as this indicates propagation to the far end of the basin from the meltwater injection location; we note that the Southern Hemisphere dynamic sea level is exactly equal and opposite by definition.

Finally, for some metrics, we quantify the change over perturbed model runs. To do this, we perform a linear fit starting from year 100 of the timeseries, and we compute the value at the final year with associated uncertainty (e.g., at year 200) utilizing this linear trend and its standard error. The assumption of a linear trend after the first 100 years of adjustment is based on the rationale that although the initial adjustment to perturbations is nonlinear, the longer-term adjustment tends to be approximately linear (e.g., see Figure A1 in the Appendix for timeseries of Northern Hemisphere dynamic sea level in response to meltwater input). The linear fit approach avoids issues due to internal variability that can arise, for example, when taking the mean over the last few decades.

3. Results

a. Variations in control ocean states

As designed, the parameter and resolution modifications in the ocean model, described in Section 2, result in a range of different ocean states. These effects are summarized using the streamfunction strengths in Figure 2. Here, we find that the $\frac{1}{4}^\circ$ simulation has a stronger upper cell MOC and a slightly weaker abyssal cell compared to the default state of the model (1° with default parameter values shown in Figure 1b and d). For the 1° set-ups, we find that the range of different states due to changing κ_v is larger than the range generated due to changing the $\kappa_{GM/Redi}$ values, including the impact on both the upper and abyssal cell strength. Increasing κ_v strengthens both the upper (as also seen in Huber and Zanna 2017) and abyssal cells (see also Figure 3). The strengthening of the abyssal cell with κ_v is consistent with Nikurashin and Vallis (2011) and Stewart et al. (2014) who argue that the cell strengthens with increased κ_v due to an advective-diffusive balance. Increasing $\kappa_{GM/Redi}$ results in a strengthened upper cell and small variations in the abyssal cell strength. This result for the upper cell is counter to Marshall et al. (2017); Saenko et al. (2018); Huber and Zanna (2017), which in global model set-ups have found that increasing the GM parameter *decreases* the MOC strength. Given our simplified model set-up and forcing profiles, it is likely that there are different controls on the strength of the overturning circulation here compared to realistic geometry. In particular, we see that the bolus streamfunction, corresponding to the contribution from the GM parameterization, follows the expected response in the Southern Ocean (e.g., Saenko et al. 2018) – namely, the strength of the bolus streamfunction increases with increasing $\kappa_{GM/Redi}$ (see Figure S1 in the Supplementary Materials). However, the increase in the residual MOC strength with larger $\kappa_{GM/Redi}$ appears to be driven by a stronger contribution at the deep water formation site at the northern edge of the basin, which may be linked to simplified boundary conditions and a lack of any imposed wind driven Ekman transport in this location. Despite this, we continue to use the simulations ranging $\kappa_{GM/Redi}$ as they behave as expected in the Southern Ocean, which is key for this study due to the location of meltwater input. Additionally, these simulations contribute to the broad goal of generating a range of background states to identify physical dependencies.

The ocean stratification changes such that larger κ_v typically leads to a decrease in stratification in the upper ocean (top ~100 meters in the midlatitudes) and an increase in stratification below that. In the Southern Ocean, the decrease in upper ocean stratification (and vice versa for smaller vertical diffusivities) extends deeper, down to ~800 meters. These general trends have complex structures with additional changes at depth that have latitudinal dependence (Figure B1 in the Appendix). Changes to the $\kappa_{GM/Redi}$ parameter values result in smaller changes in the stratification compared to changing κ_v, although low values of the parameters tend to lead to an increase in the stratification in the upper Southern Ocean (e.g., Figure B1a-c). In the $\frac{1}{4}^\circ$ simulation, we find a weaker stratification near the surface and stronger stratification below that in the midlatitudes compared to the default 1° model; in the Southern Ocean, we

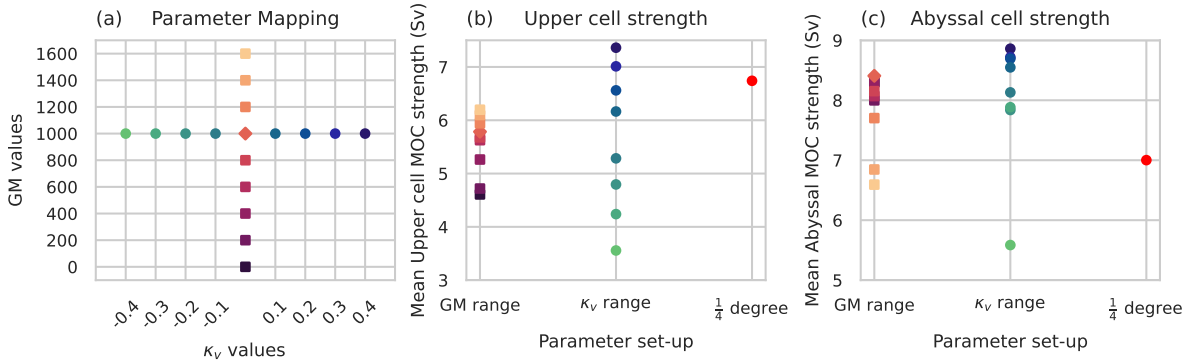

FIG. 2. The circulation strength in the control simulations for the perturbed parameter ensemble. (a) the parameter ranges as indicated in Figure 1 along with the associated colors used; (b) the upper cell overturning strength; (c) the lower cell overturning strength.

find stratification changes in the upper ocean which are dependent on the latitude and have a complex vertical structure.

Overall, we find that these simulations sample a relatively wide spread of distinct possible states by changing the ocean model parameter values and resolution. This is indicated by the spread in the upper cell MOC, for example, where the strength in the default 1° model was 5.78 Sv and the sampled range has limits of 3.56 and 7.36 Sv; thus, the maximum spread from the default parameter values is 38% (37% compared to the ensemble mean). This is comparable to the AMOC range sampled in Huber and Zanna (2017) due to differing parameter values of 34%. It is also comparable to the spread in CMIP6, which is 34% compared to the ensemble mean (calculated from Figure 1 of Nayak et al. 2024). The perturbed parameter ensemble also samples spread in the abyssal MOC and the stratification.

b. Dynamic sea level responses to meltwater

The response of the dynamic sea level in the Northern Hemisphere to meltwater perturbations for each model set-up is shown in Figure 4a. We find that perturbations at depth result in smaller responses at the far end of the basin from the input (at 200 years) compared to surface perturbations, consistent with Eisenman et al. (2024). In particular, for any individual ocean model parameter set-up, we find that the Northern Hemisphere dynamic sea level response to a surface perturbation is more positive than the response to a deep perturbation, indicated by all points lying below the identity line in Figure 4b. This dynamic sea level pattern is nearly entirely from the steric component and the larger responses in the Northern Hemisphere to surface perturbations (i.e., more globally uniform sea level) is linked specifically to the upper ocean steric contribution (see Figure S2 in the Supplementary Materials). We stress that the sea level adjusts rapidly around the basin through the (largely globally uniform) barotropic response, but the emergence of the pattern of sea level change is through the slower baroclinic/steric response.

We find substantial spread in the resultant dynamic sea level pattern linked to the parameter set-up of the ocean model alone. This spread leads to overlap in the distributions of sea level change associated with surface versus deep meltwater input, such that Northern Hemisphere dynamic sea level changes of approximately –2 to –3cm at year 200 could result from either forcing depth, depending on the model configuration. The ensemble-mean dynamic sea level response in the Northern Hemisphere (or equivalently, the negative of the Southern Hemisphere change) is -1.45 ± 0.67 cm for surface perturbations and -3.21 ± 0.54 cm for deep perturbations.

As discussed in Section 3a, the parameter and resolution changes substantially altered the background state of the ocean. In our experiments with surface meltwater input, there is a positive relationship ($R = 0.94$) between the near-surface stratification (at 10m depth) in the Southern Ocean and the dynamic sea level response at the opposite end of the basin (Figure 5a). We hypothesize that simulations with stronger near-surface Southern Ocean stratification, in the region where sloping isopycnals leads to subduction into the pycnocline, results in injected meltwater subducted to a shallower depth in the low latitudes (and vice versa with weaker stratification). This hypothesis is visible in Figure C1, which shows the difference in zonally averaged density between the surface perturbation experiment and the control experiment. In experiments with faster adjustment (i.e., lower vertical

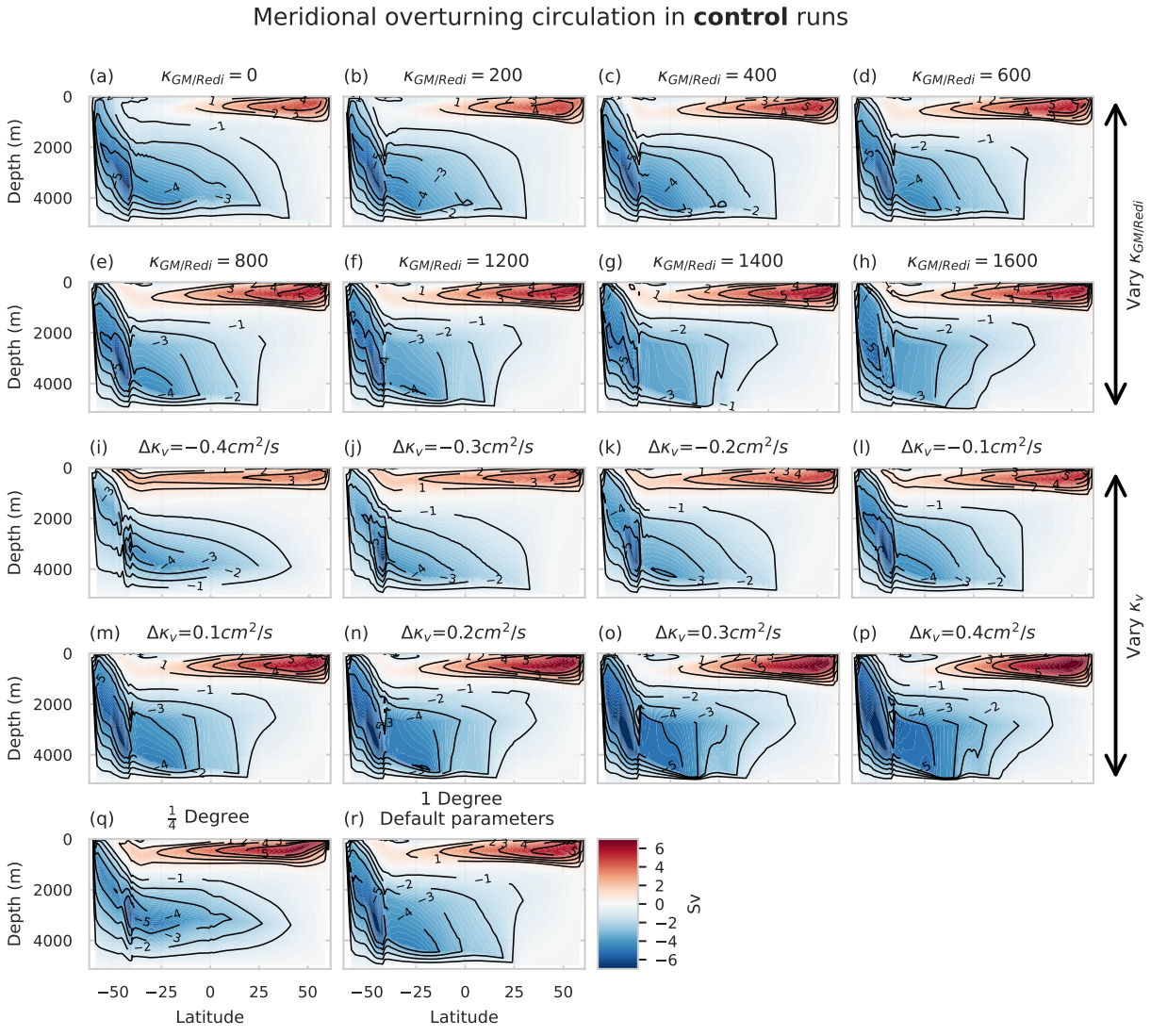

FIG. 3. Meridional overturning streamfunction in the control runs: (a)-(h) with varying GM/Redi parameter ($\kappa_{\text{GM}}, \kappa_{\text{Redi}}$) as indicated in Figure 1b, with the parameter value indicated in each subplot title; (i)-(p) changing the vertical diffusivity as indicated in Figure 1d, with the value in the subfigure title indicating the shift from the default profile (uniformly over the whole depth); (q): the $\frac{1}{4}^\circ$ run; and (r): the 1-degree run with default parameter values (see Figure 1).

diffusivities, as in panels i and j), the lower density waters associated with the meltwater stay closer to the surface both in the Southern Ocean and as they enter the low latitudes, while in experiments with slower adjustment (higher vertical diffusivities, panels o and p), the lower density water is more spread out and at lower depths. The resultant faster adjustment of model set-ups where the perturbation remains close to the surface is consistent with theoretical arguments proposed in Basinski-Ferris et al. (2025) using a reduced gravity model, constructed to represent dynamics outside the Southern Ocean, which highlighted that faster baroclinic Rossby waves near the surface can help explain faster adjustment of the upper ocean with shallower volume perturbations compared to deeper perturbations.

In the case of meltwater injected at depth, the meltwater input is statically unstable and triggers convection, ultimately being spread throughout the top 1000 meters between 60S and 50S (see Figure 7, discussed more in Section 3c). Thus, examining the stratification just near the input depth as we did in the surface perturbation experiment is not physically well motivated, as it is unclear what depth of stratification is relevant for determining

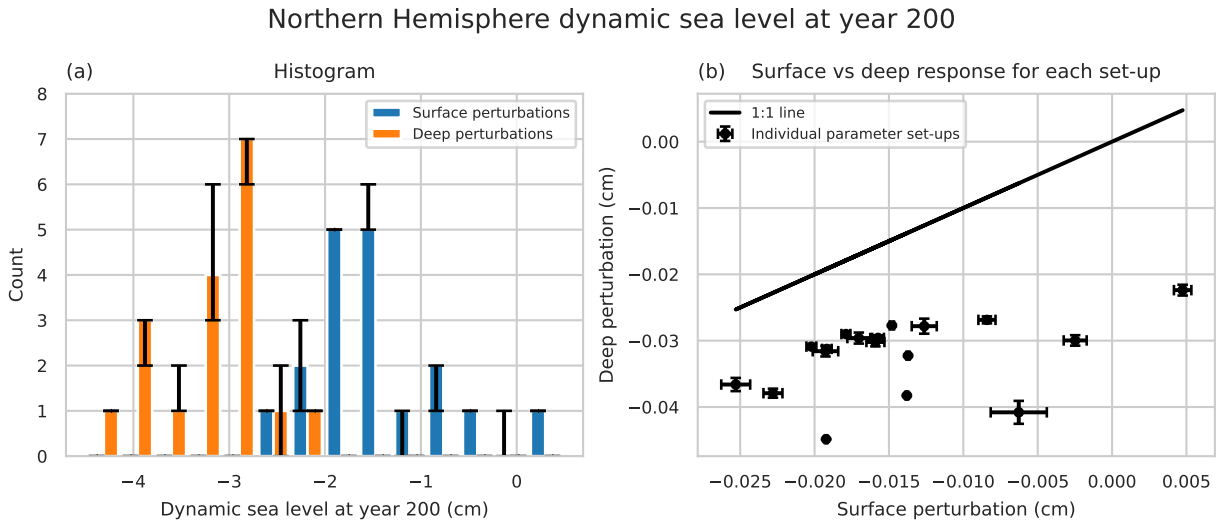

FIG. 4. Northern Hemisphere mean dynamic sea level at year 200. By definition, an equivalent plot for the Southern Hemisphere would be the exact negative of these results. All values at year 200 are estimated, with associated uncertainty (denoted with the black bars), using a linear trend fit to the timeseries of Northern Hemisphere dynamic sea level between years 100 and 200; this period corresponds to approximately linear behavior, as described in Section 2d. (a): A histogram of Northern Hemisphere dynamic sea level (with error) for each experiment. (b): Scatter plot of the Northern Hemisphere dynamic sea level in the surface perturbation experiment versus the deep perturbation experiment for each model parameter set-up; all individual points fall below the 1:1 line, indicating that for a given model set-up, the response at the opposite end of the basin from the injection location is always larger in a surface perturbation experiment than in a deep perturbation experiment.

the depth at which meltwater gets subducted into the pycnocline. We examine the simplest metric of the mean stratification over the upper ocean (top 1000 meters) and find a weak positive correlation (R=0.32) between the dynamic sea level response and the mean buoyancy frequency (Figure 5b), implying that there is not as clear of a connection between the background stratification and the spread of responses as in the surface perturbation experiment.

While we have focused on discussing correlations with stratification and proposed mechanisms that could lead to that correlation, a more thorough mechanistic proof-of-processes is necessary. In particular, cross-correlations can be present between different metrics of the ocean state such as the AMOC strength, the Southern Ocean stratification, or the dynamics of eddies; these cross-correlations can lead to different drivers identified for quantities of frequent investigation (e.g., ocean heat uptake efficiency; Winton et al. 2014; Saenko et al. 2018; Liu et al. 2023; Newsom et al. 2023). In our case, for example, the Northern Hemisphere sea level is additionally anti-correlated with the control state AMOC strength for both depths of perturbation (R values of -0.67 and -0.70 for a surface and deep perturbation respectively), despite different directions of background AMOC flow at each depth (Figure S3 in the Supplementary Materials). Thus, other correlations are present in our model simulations, which also highlight the dependence of ocean adjustment on the background state, but need to be separated to make causal arguments.

c. Ocean Circulation Responses

The most robust response to the surface meltwater forcing is a near total shutdown of the abyssal cell, due to stabilized stratification near the ocean surface which limits deep water formation; this behavior has been noted in previous studies of the response to Antarctic meltwater input (e.g., Lago and England 2019; Li et al. 2023a; Moon et al. 2025). The timeseries of the abyssal MOC strength for surface input experiments (Figure 9a and c) show consistent abyssal MOC strength reduction over the first 100-150 years with no recovery after this period of weakening. This holds for all set-ups, but there is quantitative dependence on the κ_v and $\kappa_{GM/Redi}$ values used. In particular, runs with a weaker abyssal cell in the control run tend to weaken less. For example, the lowest vertical diffusivity run, which also had the weakest control abyssal circulation, weakens much less than the other runs (see also Figure 6).

Meltwater forcing at depth also induces substantial changes in the abyssal cell. However, rather than a near shutdown of the circulation, as in the case of surface meltwater input, the abyssal cell is maintained. As in

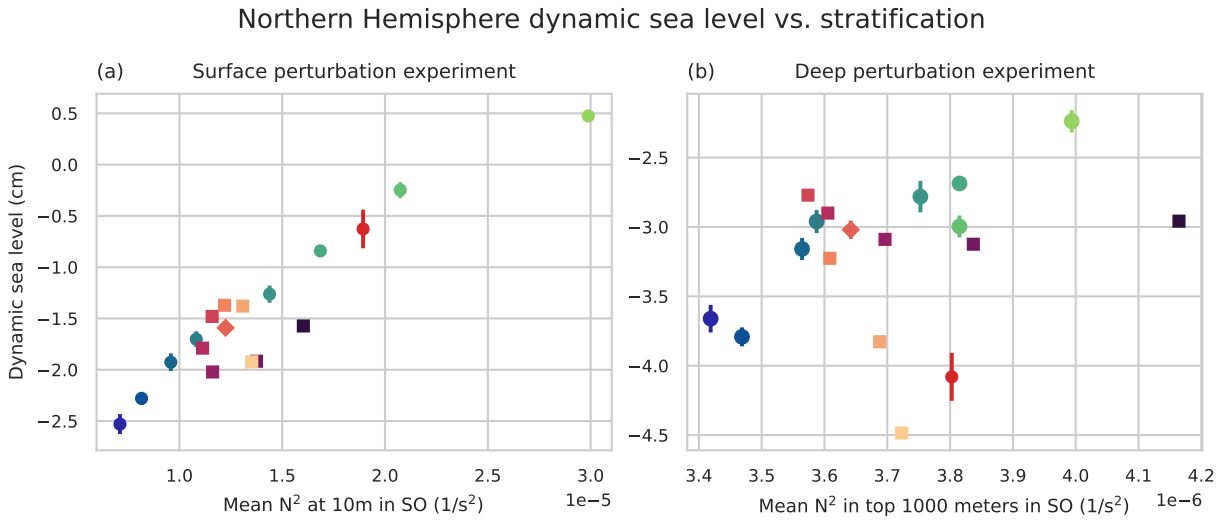

FIG. 5. Relationship between the Southern Ocean (SO) stratification (N^2), defined between 62S (the continental shelf) and 45S and the Northern Hemisphere dynamic sea level response at year 200. The color coding is as defined in Figure 2a. (a): Relationship between the dynamic sea level response to a surface meltwater perturbation and the near-surface (10 m depth) stratification in the control run in the SO. The correlation is $R = 0.94$. (b): Relationship between the dynamic sea level response to a deep meltwater perturbation and the mean stratification in the top 1000m in the control run in the SO. The correlation is $R = 0.32$. Note that an equivalent plot for the Southern Hemisphere would be the same except with the negative of the values on the y-axis.

the control simulation, the abyssal cell is closed by the formation of deep water, which in our simulations occurs at the southern-most latitudes with approximate zonal uniformity. However, the outcropping region is much smaller than in the control simulation and is not visible in the streamfunction as plotted, because it narrowly occurs along the continental shelf.

In the deep perturbation runs, the dynamics closing the abyssal cell differ substantially from the control simulations. In the control simulations, the scaling of the abyssal cell follows theories such as Nikurashin and Vallis (2011), where the steady-state residual overturning is understood through a match of approximate adiabatic dynamics in the Southern Ocean channel and diabatic dynamics in the basin, resulting in an advective-diffusive balance. In the case of fixed surface fluxes, as in our case, Stewart et al. (2014) demonstrated that with assumptions of small diffusive overturning in the channel, the streamfunction scales monotonically with small κ_v. However, in the case of the adjustment to deep meltwater input, the dynamics vary significantly from the control case because the introduction of meltwater at depth causes a large amount of mixing (through convective adjustment) and the dynamics in the channel are transient and diabatic. In the case of the deep perturbation experiment, isopycnals no longer outcrop due to a balance of Ekman transport and baroclinic instability, but instead there is a narrow outcropping region driven by the plume of meltwater which mixes throughout the upper ocean and rises. While this spatial structure is consistent between simulations, the strength of the abyssal MOC after meltwater introduction varies between ocean model set-ups (Figure 9b and d), especially dependent on κ_v as in the control circulation. Given the dynamics driving the abyssal cell in the case of deep meltwater introduction, the transient adjustment of the strength of the cell is related to how much water outcrops at the surface and interacts with surface fluxes to create deep water. This should be related to the stratification, as mixing only occurs for a convectively unstable profile, which may occur up to the surface more easily in a weakly stratified column. This is demonstrated in Figure 8, which compares the abyssal cell strength change and the control stratification near the injection location (R of -0.69). Finally, we note that there is temporal structure in the adjustment with an initial strengthening and then weakening, likely because the accumulation of meltwater freshens the Southern Ocean (Figure C2) and thereby decreases the instability of injecting additional meltwater at depth.

The changes in the upper cell in the meltwater injection simulations are smaller than the changes in the abyssal cell. In a surface perturbation experiment, the upper cell extends further south, generating a positive circulation, which is more pronounced for low $\kappa_{GM/Redi}$ values, in the

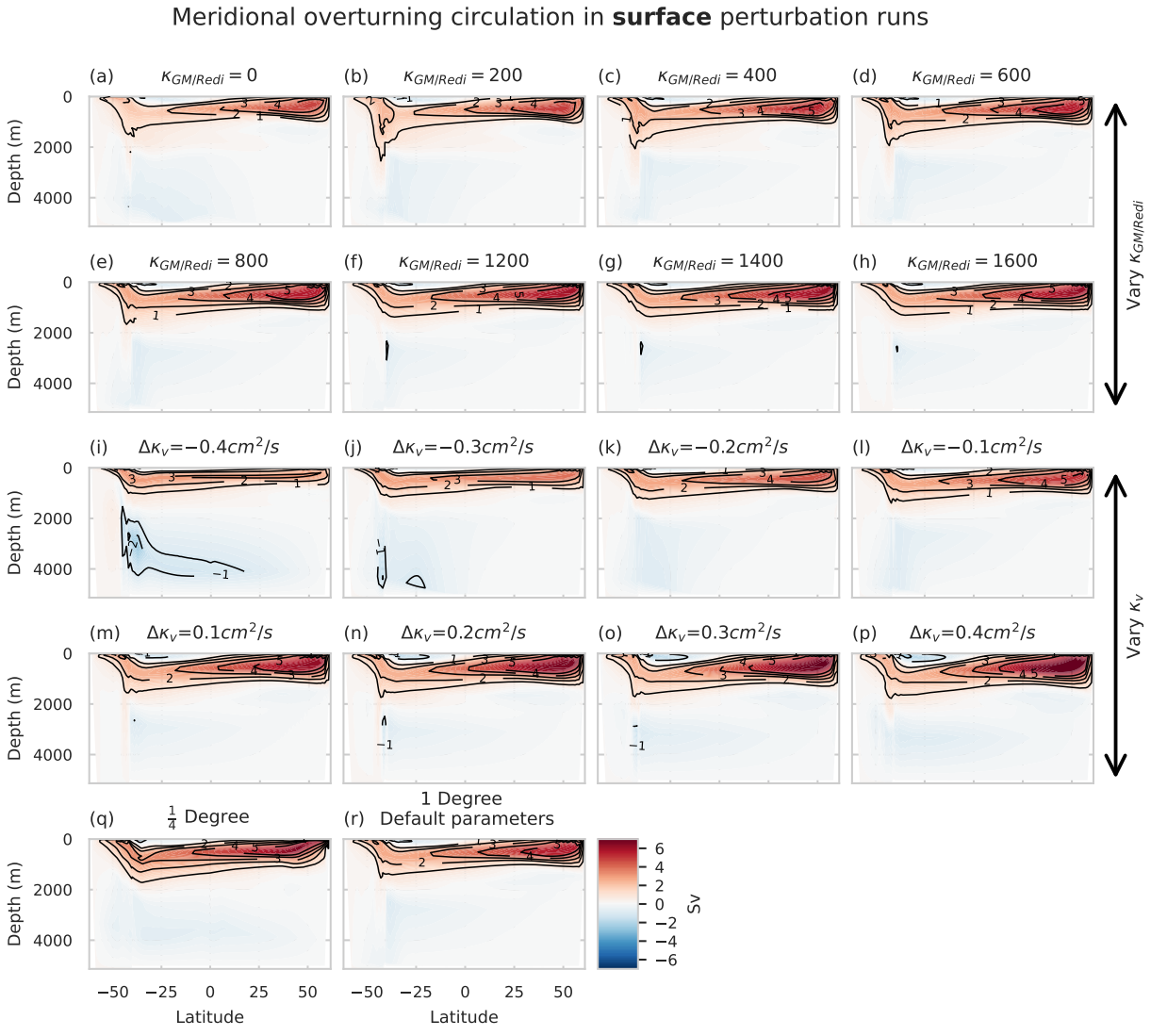

FIG. 6. Meridional overturning streamfunction in the surface perturbation runs: (a)-(h) with varying GM/Redi parameter ($\kappa_{\rm GM}$, $\kappa_{\rm Redi}$) as indicated in Figure 1b, with the parameter value indicated in each subplot title; (i)-(p) changing the vertical diffusivity as indicated in Figure 1d, with the value in the subfigure title indicating the shift from the default profile (uniformly over the whole depth); (q): the $\frac{1}{4}^\circ$ run; and (r): the 1-degree run with default parameter values (see Figure 1).

upper Southern Ocean which extends back to the continental shelf, rather than being confined to north of 40S as in the control simulations (Figure 6). The extended upper cell visible in the streamfunctions is a result of the abyssal cell (negative circulation) not outcropping in the Southern Ocean and may also be linked to increased export of water associated with meltwater input. Across model set-ups, there are differences in the strength and depth of the upper cell as it extends into the northern part of the basin, which are correlated with the upper cell in the control state (Figure 6); weaker control state MOCs for different κ_v values tend to lead to more weakening under forcing, but the relative change compared to the control overturning is small for all set-ups (less than 15% change). In the deep perturbation experiment, the upper cell extends further south than in the control simulation, and it is present at all latitudes north of the plume closing the abyssal cell (Figure 7). However, there is a substantially different structure than in the surface perturbation experiment (compare to Figure 6), with a positive streamfunction in the Southern Ocean indicating that meltwater input at depth rises close to the surface between approximately 60S and 50S. Outside of the Southern Ocean, in the midlatitudes in the Southern

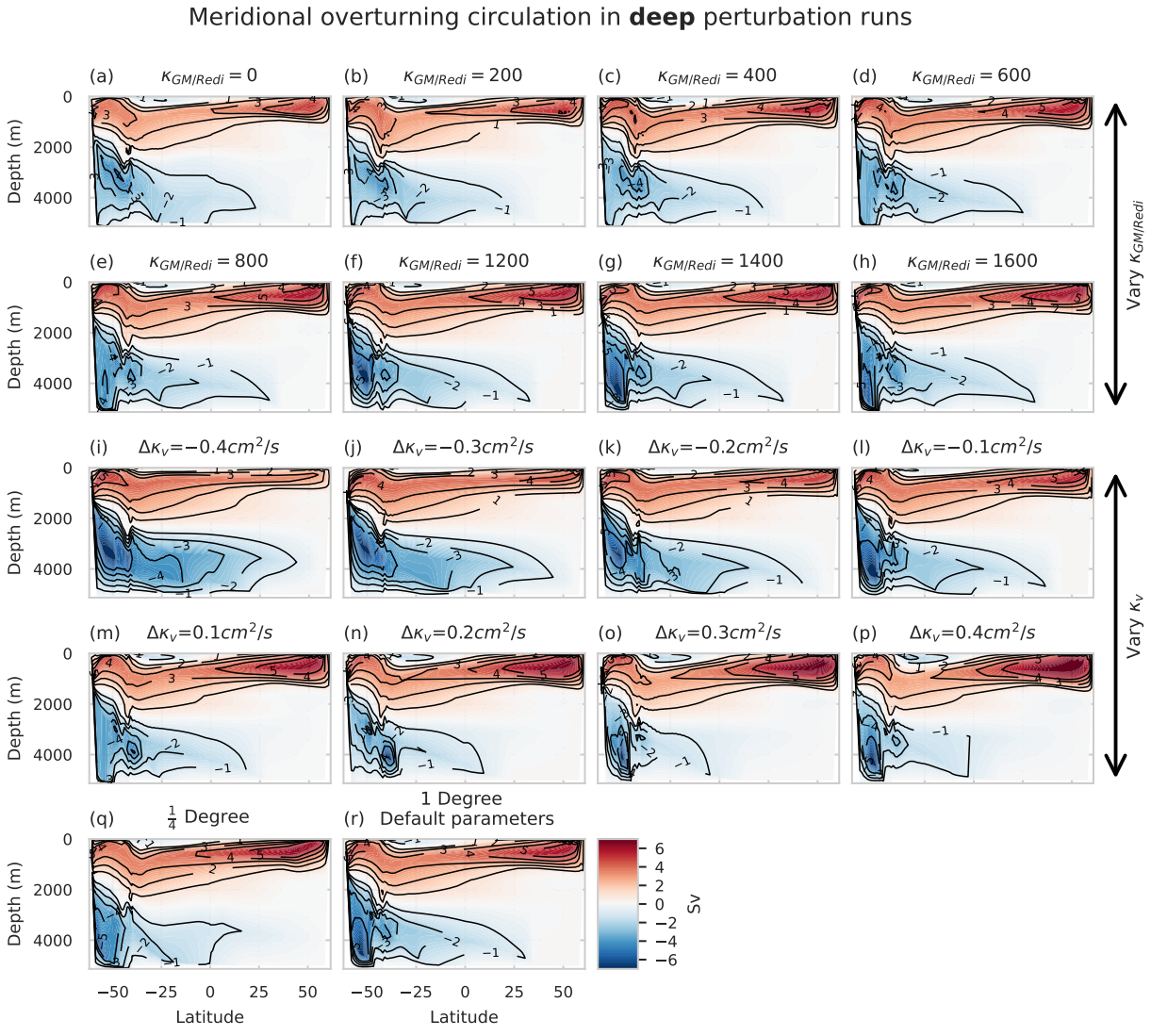

FIG. 7. Meridional overturning streamfunction in the deep perturbation runs: (a)-(h) with varying GM/Redi parameter (κ_{GM}, κ_{Redi}) as indicated in Figure 1b, with the parameter value used indicated in each subplot title; (i)-(p) changing the vertical diffusivity as indicated in Figure 1d, with the value in the subfigure title indicating the shift from the default profile (uniformly over the whole depth); (q): the $\frac{1}{4}^{\circ}$ run; and (r): the 1-degree run with default parameter values (see Figure 1).

Hemisphere, the upper cell is much deeper than in the case of a surface perturbation experiment.

4. Discussion

As mass loss from ice sheets, including Antarctica, is projected to continue over the next century (e.g, Naughten et al. 2023), understanding and correctly representing the ocean dynamic response is important for projections of a range of key climate variables. This includes the regional response of sea level (e.g., Stammer 2008; Lorbacher et al. 2012; Kopp et al. 2010; Schmidt et al. 2023), as well as the response of large-scale ocean circulation systems (e.g., Lago and England 2019; Li et al. 2023a; Moon et al. 2025), and potentially the coupled climate response including impacts on global mean temperature change (e.g., Dong et al. 2022; Bronselaer et al. 2018; Armour et al. 2024).

In this study, we have presented an investigation of potential controls on differing ocean responses to meltwater input. We have used an idealized set-up to create a perturbed parameter ensemble with 18 different configurations, including a resolution change, to partially address parameteric and structural model uncertainty.

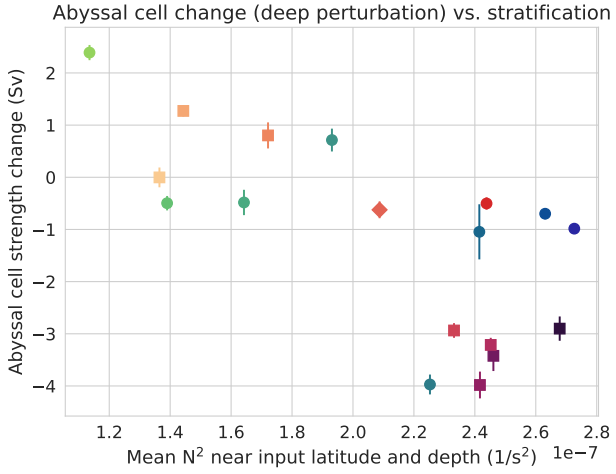

FIG. 8. Change in the abyssal cell strength in the deep perturbation runs compared to the stratification near the injection depth and location in the control simulation. The color coding is as defined in Figure 2a. We evaluate the mean from 650 meters depth to 1150 meters depth (based on the grid spacing in the vertical) and from the continental shelf to 55S.

Given that the model representation of ocean circulation is sensitive to grid resolution and physical parameter values, this ensemble allows us to identify controls on the range of ocean responses to meltwater input that may be linked to the ocean background state alone. We have additionally included idealized meltwater input at two depths due to uncertainty in how meltwater is distributed and motivated by previous work demonstrating a strong sensitivity of the ocean response to the depth of meltwater injection (Eisenman et al. 2024; Basinski-Ferris et al. 2025). Taken together, we investigate potential important controls on the range of ocean responses to Antarctic meltwater, including uncertainty that may be introduced in projections from both the model ocean state and from interfacing the ocean model with ice sheet fluxes.

For a range of ocean model parameter values, we have shown that, as in Eisenman et al. (2024), the ocean's response to meltwater forcing is highly dependent on the depth of input. In the case of the sea level adjustment, the two depths of meltwater perturbation largely resulted in distinct distributions of Northern Hemisphere dynamic sea level. In particular, for any given ocean model set-up, the surface meltwater input adjusted more quickly around the basin than deep meltwater input. Similarly, the abyssal cell, which changes substantially in response to meltwater injection, is strongly dependent on the depth of the meltwater input. In the case of surface meltwater injection, the cell nearly shuts down due to stabilized stratification near the surface preventing outcropping. For deep meltwater input, the dynamics in the Southern Ocean are diabatic and the circulation is closed by convection to the surface driven by the statically unstable injection of water into the column; thus the cell closes, albeit with significantly different dynamics than in the control simulations.

The ocean response also depends on physical parameter values such as vertical and eddy diffusivities, as well as model resolution, for both depths of meltwater injection. The adjustment of dynamic sea level across the basin has substantial spread depending on the configuration of the model. In the case of the surface input simulation, this is strongly correlated with the background stratification of the Southern Ocean, which is consistent with the hypothesis that this stratification is related to the subduction of meltwater into the pycnocline in low latitudes. In particular, stronger near-surface stratification results in meltwater remaining closer to the surface and faster adjustment, potentially related to the baroclinic Rossby wave speed, as highlighted in Basinski-Ferris et al. (2025). Similarly, in simulations where the abyssal cell is maintained (i.e., meltwater input at depth), the change in the cell is strongly dependent on the ocean model parameter set-up. We hypothesize that this is due to the new diabatic dynamics which close the cell, such that the amount of static instability of the meltwater input is linked to the background density profile. We demonstrate that more strongly stratified water columns (in the control state) near the injection location are correlated to a weakening of the abyssal cell while weakly stratified columns are correlated to a strengthening of the abyssal cell. In both cases, we stress that given the cross-correlated metrics of the ocean state, other metrics may also be correlated with the resultant sea level or abyssal cell change, necessitating additional studies aimed at determining causality rather than correlation. However, we have presented evidence that there are drivers of spread of the ocean response to meltwater depending on how the ocean model is configured and the background state that is captured, which may translate to sensitivities in more realistic models. This result for meltwater propagation adds to broader literature which has demonstrated that forced responses can be understood or constrained based on the background state, including for ocean heat uptake (e.g., Newsom et al. 2023; Liu et al. 2023; Bourgeois et al. 2022) and changes in the Atlantic MOC (e.g., Gregory et al. 2005; Bonan et al. 2025). Our results regarding the sensitivity of response to Antarctic meltwater depending on the background state and stratification may also have implications for the modelled ocean state in paleoclimate simulations aimed as a possible future analog (e.g., mid-Pliocene simulations in Haywood et al. 2020; Weiffenbach et al. 2024)

This work should be considered in the context of previous studies of the coupled climate response to meltwater

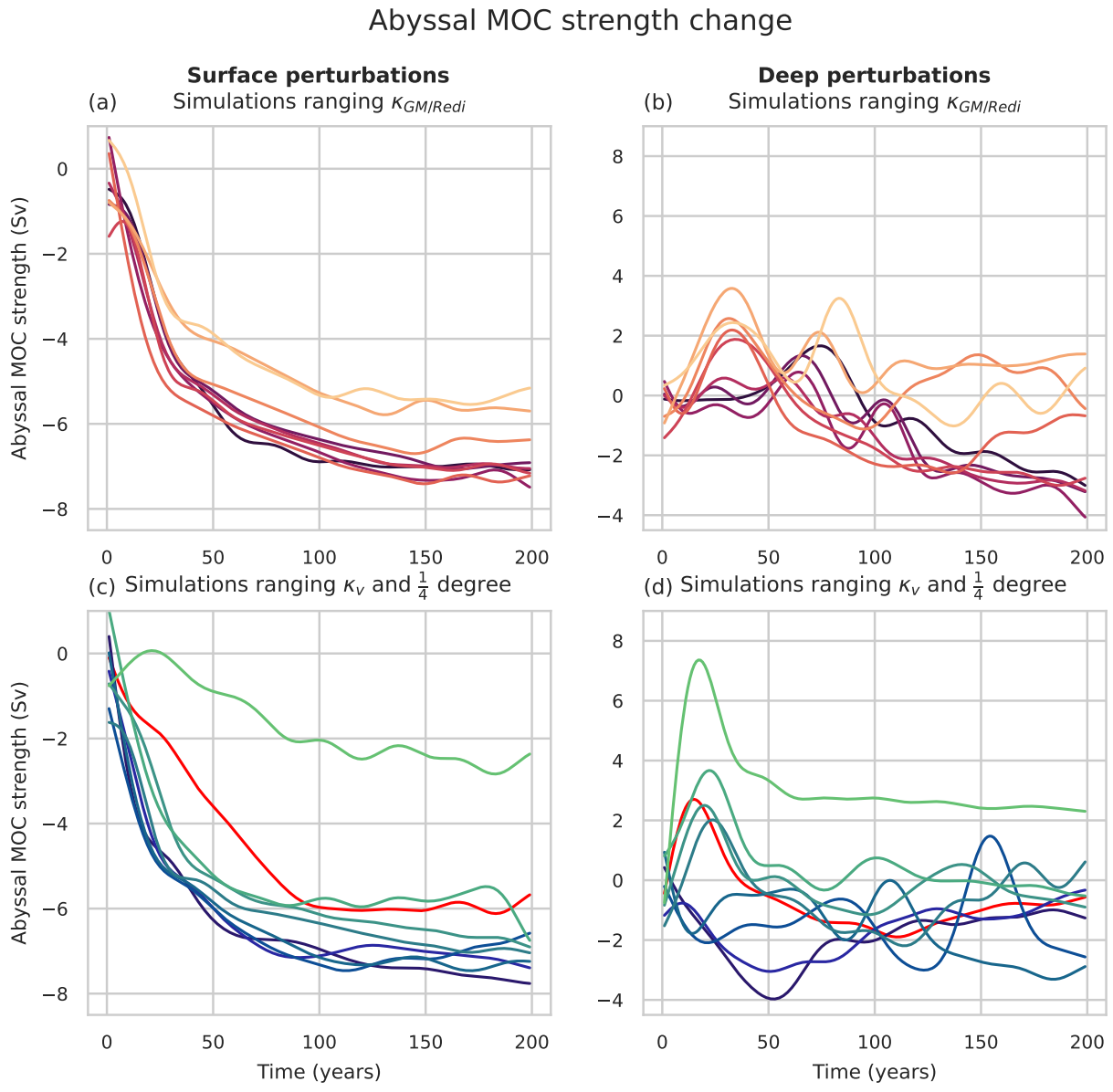

FIG. 9. The strength of the abyssal cell in response to meltwater perturbations compared to the control. The color coding is as defined in Figure 2a. Panels (a) and (c) at the surface; (b) and (d) at depth. Curves are smoothed with a 6th order low-pass Butterworth filter with a cut-off period of 30 years. The top row (a and b) are for different $\kappa_{GM/Redi}$ parameters and the bottom row (c and d) are for varying κ_V. The $\frac{1}{4}^\circ$ results are shown in (c) and (d). Here, we consider the MOC *change*, obtained by subtracting the mean of the appropriate control run. As in Figure 2, the abyssal MOC strength is found for the absolute value (so negative here in the change plot means a weakening).

input. Antarctic meltwater has been demonstrated to induce a robust response in many components of the climate system, including affecting sea ice extent and global mean surface temperature changes (e.g., Ma and Wu 2011; Bronselaer et al. 2018; Dong et al. 2022; Li et al. 2023b; Sadai et al. 2020). These responses are linked to the changed Southern Ocean stratification and heat uptake (e.g., Bronselaer et al. 2018; Dong et al. 2022; Li et al. 2023b) amongst other factors. Thus, the dependence of stratification changes on meltwater injection depth and ocean model set-up, as found here, may impact these results. Similarly, the uncertainty in the abyssal cell response, including the amount of deep water formation at the southern high latitudes, may impact

global mean temperature changes (e.g., Suzuki et al. 2022). However, the dynamic response captured in an ocean-only framework, as here, will not be the same as in a coupled atmosphere-ocean system where anomalous coupled feedbacks will modify surface fluxes (e.g., An et al. 2024). Thus, this study raises additional questions regarding how the identified controls on the response to meltwater may be extended to the coupled climate system and consequently affect other components.

We have presented an investigation exploring different controls on the ocean response to meltwater, including the possible dependence on the ocean model parameter values and resolution, as well as on the depth at which meltwater is prescribed. We note that this is a non-exhaustive investigation of uncertainty and this work aims to complement existing community efforts such as Swart et al. (2023). Here, we present results in a large perturbed parameter ensemble, which is only computationally feasible with simplifying assumptions, without aiming to investigate all questions surrounding meltwater injection (including magnitude, location, and best methods of prescription). The simplifications made should be explored more thoroughly in future work to understand the relevance of the results to similar experiments in full complexity coupled climate models. For example, here, we utilized a simple single-basin geometry to allow for a large number of experiments. However, the importance of multiple basins, accurate basin widths, and coastline geometry for the large-scale ocean circulation has been demonstrated (Ragen et al. 2022; Talley 2013; Thompson et al. 2016; Jones and Cessi 2016; Newsom and Thompson 2018; Sun et al. 2020). Second, the highest resolution utilized here was $\frac{1}{4}^{\circ}$, which is typically viewed as a "grey zone" resolution such that the need for and correct way to implement mesoscale eddy parameterizations is unclear (Hewitt et al. 2020). Examining higher resolution set-ups to more thoroughly test resolution dependence will strengthen our understanding of the impact of mesoscale eddies on the adjustment to Antarctic meltwater; this is particularly important as resolution can impact Southern Ocean stratification (e.g., Marques et al. 2022), which we have demonstrated as strongly correlated to the sea level response and abyssal cell change. Lastly, we highlight that we examined the impact of parametric uncertainty utilizing a one-at-a-time perturbed parameter ensemble, which excludes non-linear relationships between different parameters (e.g., Eidhammer et al. 2024).

Despite these caveats, we have demonstrated that ocean model parameter values and resolution, as well as the depth of meltwater perturbations have a strong influence on sea level adjustment, and the complex spatial and temporal structure of changes in circulation. This suggests that there are physical controls on the range of ocean responses that will be represented in model projections to meltwater input and should be identified to constrain and understand the forced response.

Acknowledgments. This work was funded by NSF OCE grants 2048576 and 2048590 and supported by the New York University IT High Performance Computing resources, services, and staff expertise. This project is supported in part by the Eric and Wendy Schmidt AI in Science Postdoctoral Fellowship, a program of Schmidt Sciences. Without implying their endorsement, we thank Andy Thompson, Emma Beer, Pavel Perezhogin, and Sam Schulz for helpful discussions on this work.

Data availability statement. By the time of publication, the simulation data and code to reproduce our analysis will be made available on Zenodo.

APPENDIX

APPENDIX A

Timeseries of dynamic sea level response

In the main text, we show the Northern Hemisphere dynamic sea level change at year 200 (see Figure 4). As described in Section 2d, the value of the dynamic sea level at year 200 with uncertainty is determined by a linear fit of the timeseries from year 100 to 200 where the adjustment is approximately linear. Here, we show the timeseries of the dynamic sea level for each experiment.

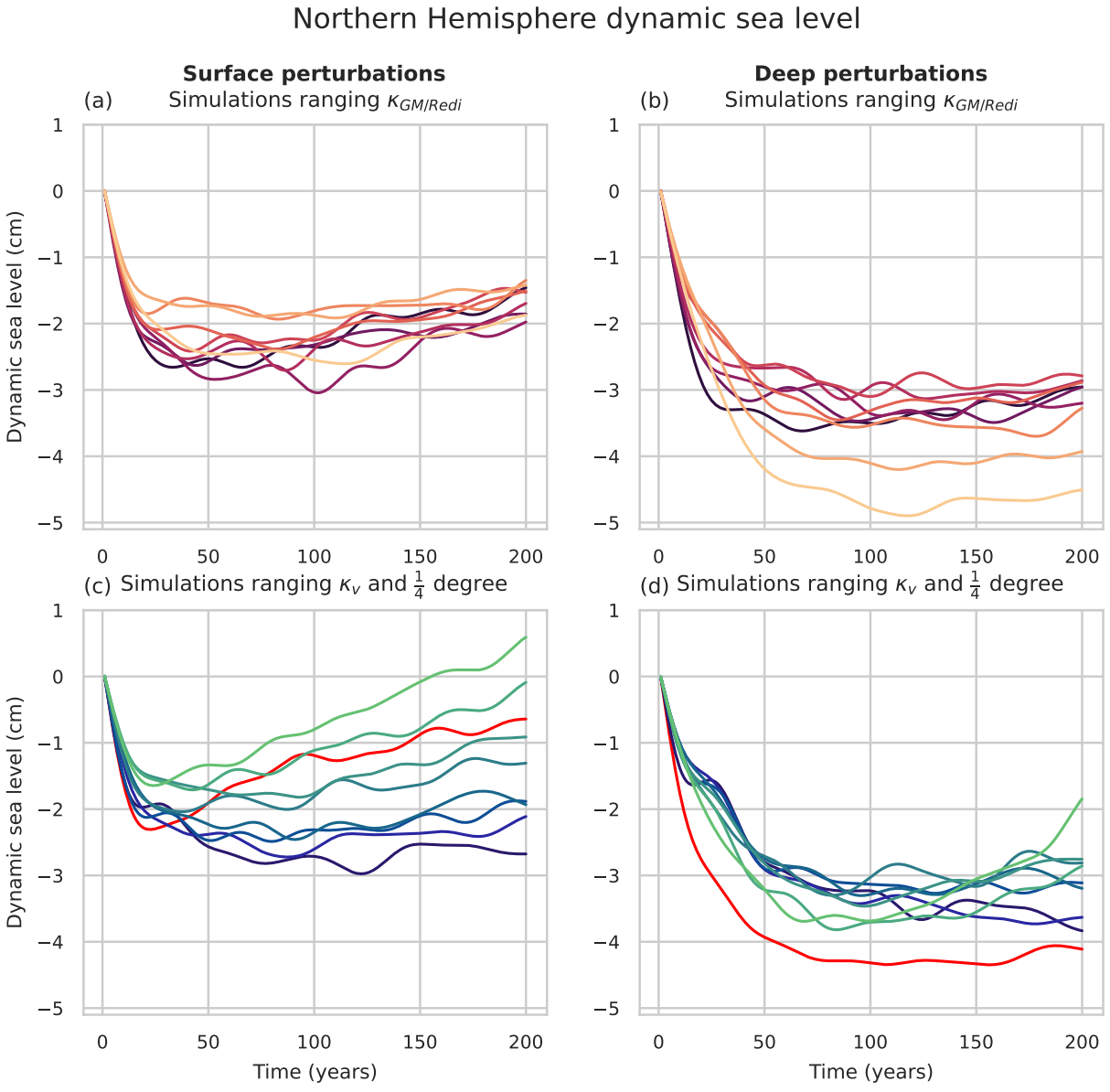

FIG. A1. Timeseries of Northern Hemisphere dynamic sea level in response to meltwater perturbations relative to control. The color coding is as defined in Figure 2a. Panels (a) and (c) at the surface; (b) and (d) at depth. Curves are smoothed with a 6th order low-pass Butterworth filter with a cut-off period of 30 years. The top row (a and b) are for different $\kappa_{GM/Redi}$ parameters and the bottom row (c and d) are for varying κ_V. The $\frac{1}{4}^\circ$ results are shown in (c) and (d). An equivalent plot for the Southern Hemisphere dynamic sea level would be the exact negative of these results by definition.

APPENDIX B

Stratification in the control simulation

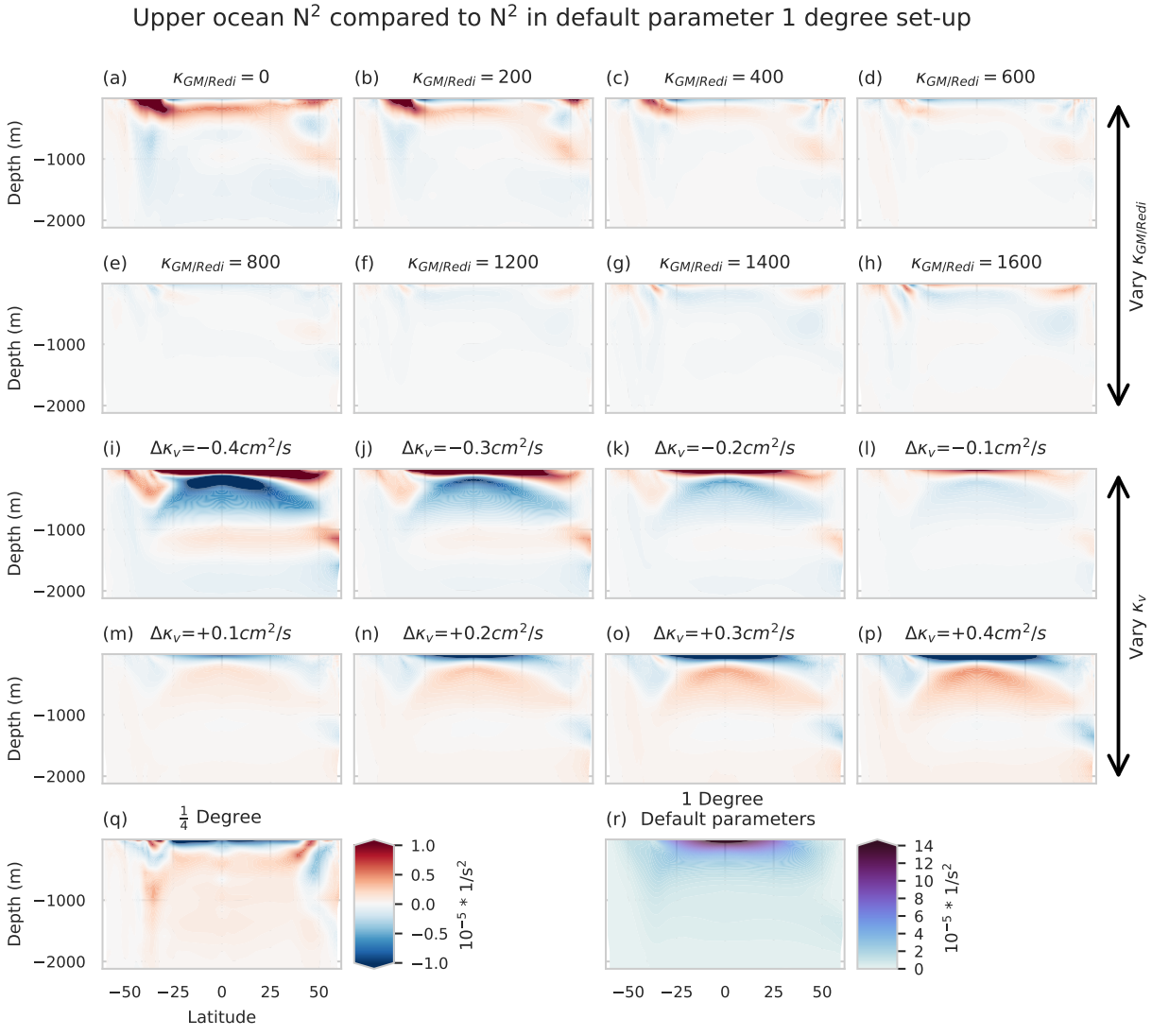

FIG. B1. Control upper ocean N^2 in each case relative to the standard 1° set-up: (a)-(h) with varying GM/Redi parameter ($\kappa_{\rm GM}, \kappa_{\rm Redi}$) as indicated in Figure 1b, with the parameter value used indicated in each subplot title; and (i)-(p) changing the vertical diffusivity as indicated in Figure 1d, with the value in the subfigure title indicating the shift from the default profile (uniformly over the whole depth); (q): the $\frac{1}{4}^\circ$ run; and (r): the 1-degree run with default parameter values (see Figure 1), i.e. the profile that is subtracted from all other set-ups.

APPENDIX C

Density change after perturbation

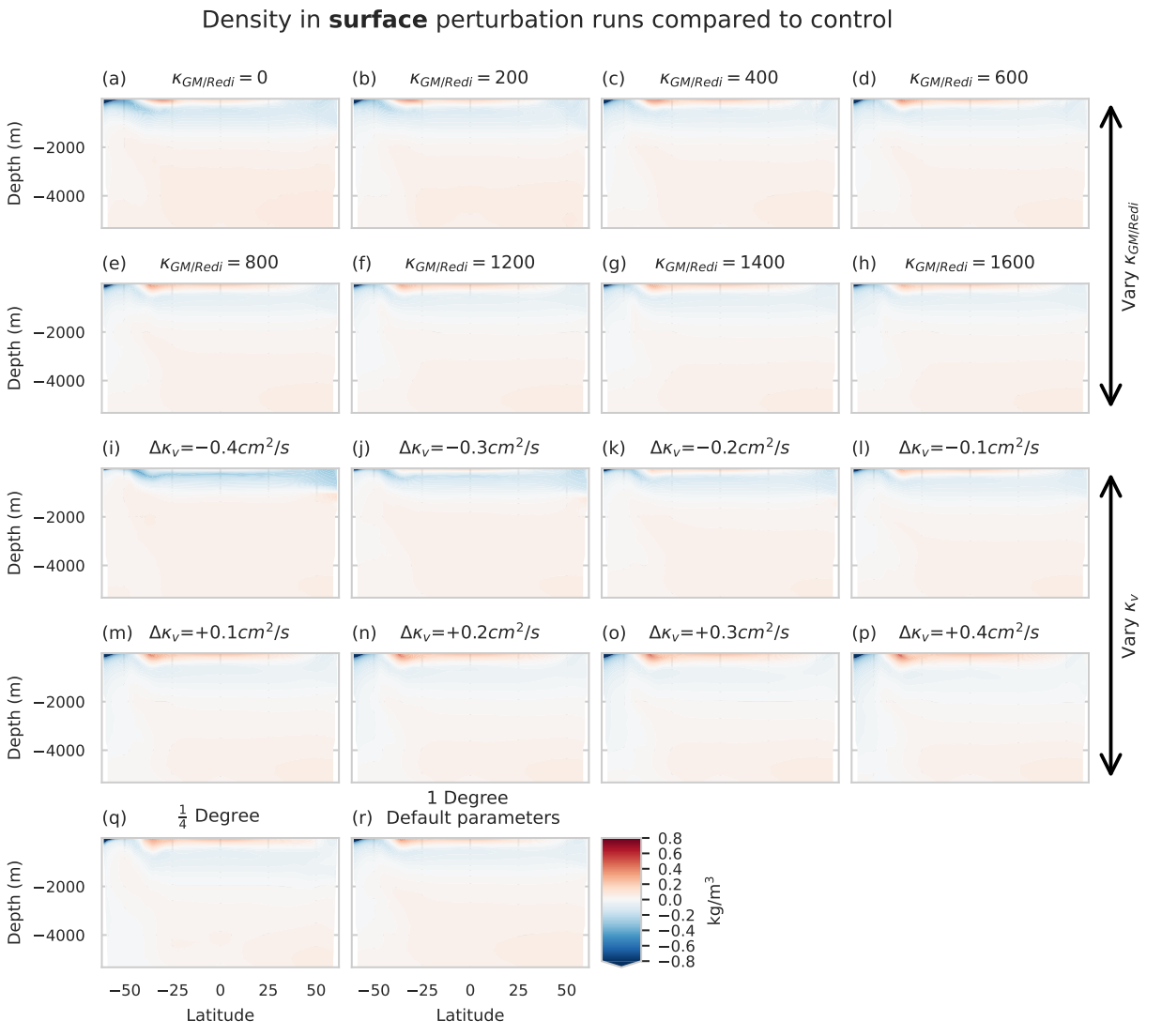

FIG. C1. Density change in a surface perturbation experiment relative to control: with varying GM/Redi parameter ($\kappa_{\rm GM}, \kappa_{\rm Redi}$) as indicated in Figure 1b, with the parameter value used indicated in each subplot title; and (i)-(p) changing the vertical diffusivity as indicated in Figure 1d, with the value in the subfigure title indicating the shift from the default profile (uniformly over the whole depth); (q): the $\frac{1}{4}^\circ$ run; and (r): the 1-degree run with default parameter values (see Figure 1). Note that for all plots, we subtract off the global mean change in density – thus, this is the anomaly (compared to the global mean) of the density change.

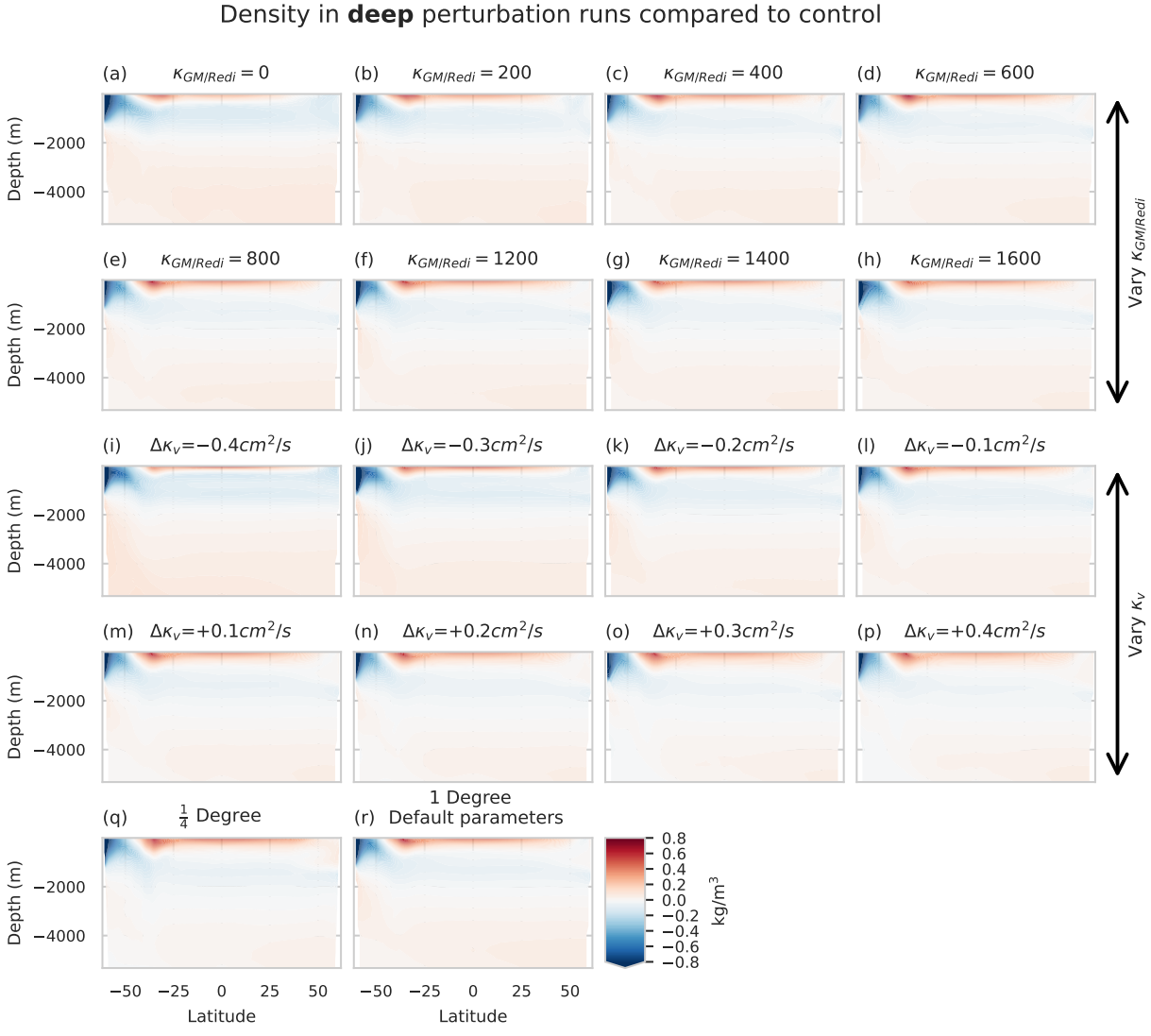

FIG. C2. Density change in a deep perturbation experiment relative to control: with varying GM/Redi parameter ($\kappa_{\rm GM}, \kappa_{\rm Redi}$) as indicated in Figure 1b, with the parameter value used indicated in each subplot title; and (i)-(p) changing the vertical diffusivity as indicated in Figure 1d, with the value in the subfigure title indicating the shift from the default profile (uniformly over the whole depth); (q): the $\frac{1}{4}^\circ$ run; and (r): the 1-degree run with default parameter values (see Figure 1). Note that for all plots, we subtract off the global mean change in density – thus, this is the anomaly (compared to the global mean) of the density change.

References

An, S.-I., J.-Y. Moon, H. A. Dijkstra, Y.-M. Yang, and H. Song, 2024: Antarctic meltwater reduces the Atlantic meridional overturning circulation through oceanic freshwater transport and atmospheric teleconnections. *Communications Earth & Environment*, **5**, https://doi.org/10.1038/s43247-024-01670-7.

Armour, K. C., and Coauthors, 2024: Sea-surface temperature pattern effects have slowed global warming and biased warming-based constraints on climate sensitivity. *Proceedings of the National Academy of Sciences*, **121 (12)**, e2312093 121, https://doi.org/10.1073/pnas.2312093121.

Arnscheidt, C. W., J. Marshall, P. Dutrieux, C. D. Rye, and A. Ramadhan, 2021: On the Settling Depth of Meltwater Escaping from beneath Antarctic Ice Shelves. *Journal of Physical Oceanography*, **51 (7)**, 2257–2270, https://doi.org/10.1175/JPO-D-20-0286.1.

Basinski-Ferris, A., L. Zanna, and I. Eisenman, 2025: A Theory for How the Depth of Meltwater Injection Impacts Regional Sea Level Evolution. *Journal of Physical Oceanography*, **55 (8)**, 1139–1154, https://doi.org/10.1175/JPO-D-24-0153.1.

Beadling, R. L., and Coauthors, 2022: Importance of the Antarctic Slope Current in the Southern Ocean Response to Ice Sheet Melt and Wind Stress Change. *Journal of Geophysical Research: Oceans*, **127 (5)**, e2021JC017 608, https://doi.org/10.1029/2021JC017608.

Bonan, D. B., A. F. Thompson, T. Schneider, L. Zanna, K. C. Armour, and S. Sun, 2025: Observational constraints imply limited future Atlantic meridional overturning circulation weakening. *Nature Geoscience*, **18**, 479–487, https://doi.org/10.1038/s41561-025-01709-0.

Bourgeois, T., N. Goris, J. Schwinger, and J. F. Tjiputra, 2022: Stratification constrains future heat and carbon uptake in the Southern Ocean between 30°S and 55°S. *Nature Communications*, **13**, https://doi.org/10.1038/s41467-022-27979-5.

Bronselaer, B., M. Winton, S. M. Griffies, W. J. Hurlin, K. B. Rodgers, O. V. Sergienko, R. J. Stouffer, and J. L. Russell, 2018: Change in future climate due to Antarctic meltwater. *Nature*, **564**, 53–58, https://doi.org/10.1038/s41586-018-0712-z.

Bronselaer, B., and Coauthors, 2020: Importance of wind and meltwater for observed chemical and physical changes in the Southern Ocean. *Nature Geoscience*, **13**, 35–42, https://doi.org/10.1038/s41561-019-0502-8.

Bryan, K., and L. J. Lewis, 1979: A water mass model of the World Ocean. *Journal of Geophysical Research: Oceans*, **84 (C5)**, 2503–2517, https://doi.org/10.1029/JC084IC05P02503.

Depoorter, M. A., J. L. Bamber, J. A. Griggs, J. T. M. Lenaerts, S. R. M. Ligtenberg, M. R. Van Den Broeke, and G. Moholdt, 2013: Calving fluxes and basal melt rates of Antarctic ice shelves. *Nature*, **502**, 89–92, https://doi.org/10.1038/nature12567.

Dong, Y., A. G. Pauling, S. Sadai, and K. C. Armour, 2022: Antarctic Ice-Sheet Meltwater Reduces Transient Warming and Climate Sensitivity Through the Sea-Surface Temperature Pattern Effect. *Geophysical Research Letters*, **49 (24)**, e2022GL101 249, https://doi.org/10.1029/2022GL101249.

Döös, K., and D. J. Webb, 1994: The Deacon Cell and the Other Meridional Cells of the Southern Ocean. *Journal of Physical Oceanography*, **24 (2)**, 429–442, https://doi.org/10.1175/1520-0485(1994)024⟨0429:TDCATO⟩2.0.CO;2.

Ehlert, D., K. Zickfeld, M. Eby, and N. Gillett, 2017: The Sensitivity of the Proportionality between Temperature Change and Cumulative CO2 Emissions to Ocean Mixing. *Journal of Climate*, **30 (8)**, 2921–2935, https://doi.org/10.1175/JCLI-D-16-0247.1.

Eidhammer, T., and Coauthors, 2024: An extensible perturbed parameter ensemble for the Community Atmosphere Model version 6. *Geoscientific Model Development*, **17 (21)**, 7835–7853, https://doi.org/10.5194/gmd-17-7835-2024.

Eisenman, I., A. Basinski-Ferris, E. Beer, and L. Zanna, 2024: The Sensitivity of the Spatial Pattern of Sea Level Changes to the Depth of Antarctic Meltwater Fluxes. *Geophysical Research Letters*, **51 (19)**, e2024GL110 633, https://doi.org/10.1029/2024GL110633.

Eyring, V., S. Bony, G. A. Meehl, C. A. Senior, B. Stevens, R. J. Stouffer, and K. E. Taylor, 2016: Overview of the Coupled Model Intercomparison Project Phase 6 (CMIP6) experimental design and organization. *Geoscientific Model Development*, **9 (5)**, 1937–1958, https://doi.org/10.5194/GMD-9-1937-2016.

Farrell, W. E., and J. A. Clark, 1976: On Postglacial Sea Level. *Geophysical Journal International*, **46 (3)**, 647–667, https://doi.org/10.1111/J.1365-246X.1976.TB01252.X.

Garabato, A. C. N., and Coauthors, 2017: Vigorous lateral export of the meltwater outflow from beneath an Antarctic ice shelf. *Nature*, **542**, 219–222, https://doi.org/10.1038/nature20825.

Gent, P. R., and J. C. McWilliams, 1990: Isopycnal Mixing in Ocean Circulation Models. *Journal of Physical Oceanography*, **20 (1)**, 150–155, https://doi.org/10.1175/1520-0485(1990)020⟨0150:IMIOCM⟩2.0.CO;2.

Golledge, N. R., E. D. Keller, N. Gomez, K. A. Naughten, J. Bernales, L. D. Trusel, and T. L. Edwards, 2019: Global environmental consequences of twenty-first-century ice-sheet melt. *Nature*, **566**, 65–72, https://doi.org/10.1038/s41586-019-0889-9.

Gregory, J. M., and Coauthors, 2005: A model intercomparison of changes in the Atlantic thermohaline circulation in response to increasing atmospheric CO2 concentration. *Geophysical Research Letters*, **32 (12)**, https://doi.org/10.1029/2005GL023209.

Haywood, A. M., and Coauthors, 2020: The Pliocene Model Intercomparison Project Phase 2: large-scale climate features and climate sensitivity. *Climate of the Past*, **16 (6)**, 2095–2123, https://doi.org/10.5194/cp-16-2095-2020.

Hewitt, H. T., and Coauthors, 2020: Resolving and Parameterising the Ocean Mesoscale in Earth System Models. *Current Climate Change Reports*, **6**, 137–152, https://doi.org/10.1007/s40641-020-00164-w.

Huber, M. B., and L. Zanna, 2017: Drivers of uncertainty in simulated ocean circulation and heat uptake. *Geophysical Research Letters*, **44 (3)**, 1402–1413, https://doi.org/10.1002/2016GL071587.

Jackett, D. R., and T. J. Mcdougall, 1995: Minimal Adjustment of Hydrographic Profiles to Achieve Static Stability. *Journal of Atmospheric and Oceanic Technology*, **12 (2)**, 381–389, https://doi.org/10.1175/1520-0426(1995)012⟨0381:MAOHPT⟩2.0.CO;2.

Jansen, M. F., L. P. Nadeau, and T. M. Merlis, 2018: Transient versus Equilibrium Response of the Ocean's Overturning Circulation to Warming. *Journal of Climate*, **31 (13)**, 5147–5163, https://doi.org/10.1175/JCLI-D-17-0797.1.

Jones, C. S., and P. Cessi, 2016: Interbasin Transport of the Meridional Overturning Circulation. *Journal of Physical Oceanography*, **46 (4)**, 1157–1169, https://doi.org/10.1175/JPO-D-15-0197.1.

Jones, D. C., T. Ito, and N. S. Lovenduski, 2011: The transient response of the Southern Ocean pycnocline to changing atmospheric winds. *Geophysical Research Letters*, **38 (15)**, https://doi.org/10.1029/2011GL048145.

Kim, I., D. Hahm, T. S. Rhee, T. W. Kim, C. S. Kim, and S. H. Lee, 2016: The distribution of glacial meltwater in the Amundsen Sea, Antarctica, revealed by dissolved helium and neon. *Journal of Geophysical Research: Oceans*, **121 (3)**, 1654–1666, https://doi.org/10.1002/2015JC011211.

Kopp, R. E., J. X. Mitrovica, S. M. Griffies, J. Yin, C. C. Hay, and R. J. Stouffer, 2010: The impact of Greenland melt on local sea levels: A partially coupled analysis of dynamic and static equilibrium effects in idealized water-hosing experiments. *Climatic Change*, **103**, 619–625, https://doi.org/10.1007/s10584-010-9935-1.

Lago, V., and M. H. England, 2019: Projected Slowdown of Antarctic Bottom Water Formation in Response to Amplified Meltwater Contributions. *Journal of Climate*, **32 (19)**, 6319–6335, https://doi.org/10.1175/JCLI-D-18-0622.1.

Leutbecher, M., and Coauthors, 2017: Stochastic representations of model uncertainties at ECMWF: state of the art and future vision. *Quarterly Journal of the Royal Meteorological Society*, **143 (707)**, 2315–2339, https://doi.org/10.1002/QJ.3094.

Li, Q., M. H. England, A. M. C. Hogg, S. R. Rintoul, and A. K. Morrison, 2023a: Abyssal ocean overturning slowdown and warming driven by Antarctic meltwater. *Nature*, **615**, 841–847, https://doi.org/10.1038/s41586-023-05762-w.

Li, Q., J. Marshall, C. D. Rye, A. Romanou, D. Rind, and M. Kelley, 2023b: Global Climate Impacts of Greenland and Antarctic Meltwater: A Comparative Study. *Journal of Climate*, **36 (11)**, 3571–3590, https://doi.org/10.1175/JCLI-D-22-0433.1.

Liu, M., B. J. Soden, G. A. Vecchi, and C. Wang, 2023: The Spread of Ocean Heat Uptake Efficiency Traced to Ocean Salinity. *Geophysical Research Letters*, **50 (4)**, e2022GL100 171, https://doi.org/10.1029/2022GL100171.

Loose, N., G. M. Marques, A. Adcroft, S. Bachman, S. M. Griffies, I. Grooms, R. W. Hallberg, and M. F. Jansen, 2023: Comparing Two Parameterizations for the Restratification Effect of Mesoscale Eddies in an Isopycnal Ocean Model. *Journal of Advances in Modeling Earth Systems*, **15 (12)**, e2022MS003 518, https://doi.org/10.1029/2022MS003518.

Lorbacher, K., S. J. Marsland, J. A. Church, S. M. Griffies, and D. Stammer, 2012: Rapid barotropic sea level rise from ice sheet melting. *Journal of Geophysical Research: Oceans*, **117 (C6)**, https://doi.org/10.1029/2011JC007733.

Luongo, M. T., N. G. Brizuela, I. Eisenman, and S. P. Xie, 2024: Retaining Short-Term Variability Reduces Mean State Biases in Wind Stress Overriding Simulations. *Journal of Advances in Modeling Earth Systems*, **16 (2)**, e2023MS003 665, https://doi.org/10.1029/2023MS003665.

Ma, H., and L. Wu, 2011: Global Teleconnections in Response to Freshening over the Antarctic Ocean. *Journal of Climate*, **24 (4)**, 1071–1088, https://doi.org/10.1175/2010JCLI3634.1.

MacDougall, A. H., N. C. Swart, and R. Knutti, 2017: The Uncertainty in the Transient Climate Response to Cumulative CO2 Emissions Arising from the Uncertainty in Physical Climate Parameters. *Journal of Climate*, **30 (2)**, 813–827, https://doi.org/10.1175/JCLI-D-16-0205.1.

Marques, G. M., and Coauthors, 2022: NeverWorld2: An idealized model hierarchy to investigate ocean mesoscale eddies across resolutions. *Geoscientific Model Development*, **15 (17)**, 6567–6579, https://doi.org/10.5194/GMD-15-6567-2022.

Marshall, J., A. Adcroft, C. Hill, L. Perelman, and C. Heisey, 1997: A finite-volume, incompressible Navier Stokes model for studies of the ocean on parallel computers. *Journal of Geophysical Research: Oceans*, **102 (C3)**, 5753–5766, https://doi.org/10.1029/96JC02775.

Marshall, J., J. R. Scott, A. Romanou, M. Kelley, and A. Leboissetier, 2017: The dependence of the ocean's MOC on mesoscale eddy diffusivities: A model study. *Ocean Modelling*, **111**, 1–8, https://doi.org/10.1016/J.OCEMOD.2017.01.001.

Mignot, J., A. Levermann, and A. Griesel, 2006: A Decomposition of the Atlantic Meridional Overturning Circulation into Physical Components Using Its Sensitivity to Vertical Diffusivity. *Journal of Physical Oceanography*, **36 (4)**, 636–650, https://doi.org/10.1175/JPO2891.1.

Mitrovica, J. X., C. C. Hay, R. E. Kopp, C. Harig, and K. Latychev, 2018: Quantifying the Sensitivity of Sea Level Change in Coastal Localities to the Geometry of Polar Ice Mass Flux. *Journal of Climate*, **31 (9)**, 3701–3709, https://doi.org/10.1175/JCLI-D-17-0465.1.

Moon, J.-Y., S.-I. An, G. Mandal, H. Song, Y.-M. Yang, and S.-E. Park, 2025: Antarctic meltwater spread pattern and its duration modulate abyssal circulation. *Communications Earth & Environment*, **6**, 586, https://doi.org/10.1038/s43247-025-02589-3.

Moorman, R., A. K. Morrison, and A. M. Hogg, 2020: Thermal Responses to Antarctic Ice Shelf Melt in an Eddy-Rich Global Ocean–Sea Ice Model. *Journal of Climate*, **33 (15)**, 6599–6620, https://doi.org/10.1175/JCLI-D-19-0846.1.

Munday, D. R., H. L. Johnson, and D. P. Marshall, 2013: Eddy Saturation of Equilibrated Circumpolar Currents. *Journal of Physical Oceanography*, **43 (3)**, 507–532, https://doi.org/10.1175/JPO-D-12-095.1.

Naughten, K. A., P. R. Holland, and J. De Rydt, 2023: Unavoidable future increase in West Antarctic ice-shelf melting over the twenty-first century. *Nature Climate Change*, **13**, 1222–1228, https://doi.org/10.1038/s41558-023-01818-x.

Nayak, M. S., D. B. Bonan, E. R. Newsom, and A. F. Thompson, 2024: Controls on the Strength and Structure of the Atlantic Meridional Overturning Circulation in Climate Models. *Geophysical Research Letters*, **51 (11)**, e2024GL109 055, https://doi.org/10.1029/2024GL109055.

Newsom, E., L. Zanna, and J. Gregory, 2023: Background Pycnocline Depth Constrains Future Ocean Heat Uptake Efficiency. *Geophysical Research Letters*, **50 (22)**, e2023GL105 673, https://doi.org/10.1029/2023GL105673.

Newsom, E. R., and A. F. Thompson, 2018: Reassessing the Role of the Indo-Pacific in the Ocean's Global Overturning Circulation. *Geophysical Research Letters*, **45 (22)**, 12 422–12 431, https://doi.org/10.1029/2018GL080350.

Nikurashin, M., and G. Vallis, 2011: A Theory of Deep Stratification and Overturning Circulation in the Ocean. *Journal of Physical Oceanography*, **41 (3)**, 485–502, https://doi.org/10.1175/2010JPO4529.1.

Oka, A., 2025: Deep ocean mixing mismatch between model and observational estimates. *Communications Earth & Environment*, **6**, 108, https://doi.org/10.1038/s43247-025-02027-4.

Oppenheimer, M., and Coauthors, 2019: Sea Level Rise and Implications for Low-Lying Islands, Coasts and Communities. *IPCC Special Report on the Ocean and Cryosphere in a Changing Climate*, H.-O. Pörtner, D. C. Roberts, V. Masson-Delmotte, P. Zhai, M. Tignor, E. Poloczanska, K. Mintenbeck, A. Alegría, M. Nicolai, A. Okem, J. Petzold, B. Rama, and N. M. Weyer, Eds., Cambridge University Press, 321–445, https://doi.org/10.1017/9781009157964.006.

Otosaka, I. N., and Coauthors, 2023: Mass balance of the Greenland and Antarctic ice sheets from 1992 to 2020. *Earth System Science Data*, **15 (4)**, 1597–1616, https://doi.org/10.5194/ESSD-15-1597-2023.

Park, J. Y., F. Schloesser, A. Timmermann, D. Choudhury, J. Y. Lee, and A. B. Nellikkattil, 2023: Future sea-level projections with a coupled atmosphere-ocean-ice-sheet model. *Nature Communications*, **14**, 636, https://doi.org/10.1038/s41467-023-36051-9.

Pritchard, H. D., S. R. M. Ligtenberg, H. A. Fricker, D. G. Vaughan, M. R. Van Den Broeke, and L. Padman, 2012: Antarctic ice-sheet loss driven by basal melting of ice shelves. *Nature*, **484**, 502–505, https://doi.org/10.1038/nature10968.

Ragen, S., K. C. Armour, L. Thompson, A. Shao, and D. Darr, 2022: The Role of Atlantic Basin Geometry in Meridional Overturning Circulation. *Journal of Physical Oceanography*, **52 (3)**, 475–492, https://doi.org/10.1175/JPO-D-21-0036.1.

Redi, M. H., 1982: Oceanic Isopycnal Mixing by Coordinate Rotation. *Journal of Physical Oceanography*, **12 (10)**, 1154–1158, https://doi.org/10.1175/1520-0485(1982)012⟨1154:OIMBCR⟩2.0.CO;2.

Rignot, E., S. Jacobs, J. Mouginot, and B. Scheuchl, 2013: Ice-shelf melting around Antarctica. *Science*, **341 (6143)**, 266–270, https://doi.org/10.1126/science.1235798.

Roberts, M. J., and Coauthors, 2020: Sensitivity of the Atlantic Meridional Overturning Circulation to Model Resolution in CMIP6 HighResMIP Simulations and Implications for Future Changes. *Journal of Advances in Modeling Earth Systems*, **12 (8)**, e2019MS002 014, https://doi.org/10.1029/2019MS002014.

Sadai, S., A. Condron, R. DeConto, and D. Pollard, 2020: Future climate response to Antarctic Ice Sheet melt caused by anthropogenic warming. *Science Advances*, **6 (39)**, https://doi.org/10.1126/sciadv.aaz1169.

Saenko, O. A., D. Yang, and J. M. Gregory, 2018: Impact of Mesoscale Eddy Transfer on Heat Uptake in an Eddy-Parameterizing Ocean Model. *Journal of Climate*, **31 (20)**, 8589–8606, https://doi.org/10.1175/JCLI-D-18-0186.1.

Schmidt, G. A., and Coauthors, 2023: Anomalous Meltwater From Ice Sheets and Ice Shelves Is a Historical Forcing. *Geophysical Research Letters*, **50 (24)**, e2023GL106 530, https://doi.org/10.1029/2023GL106530.

Stammer, D., 2008: Response of the global ocean to Greenland and Antarctic ice melting. *Journal of Geophysical Research: Oceans*, **113 (C6)**, https://doi.org/10.1029/2006JC004079.

Stewart, A. L., R. Ferrari, and A. F. Thompson, 2014: On the Importance of Surface Forcing in Conceptual Models of the Deep Ocean. *Journal of Physical Oceanography*, **44 (3)**, 891–899, https://doi.org/10.1175/JPO-D-13-0206.1.

Sun, S., A. F. Thompson, and I. Eisenman, 2020: Transient Overturning Compensation between Atlantic and Indo-Pacific Basins. *Journal of Physical Oceanography*, **50 (8)**, 2151–2172, https://doi.org/10.1175/JPO-D-20-0060.1.

Suzuki, T., Y. Komuro, K. Kusahara, and H. Tatebe, 2022: Transient Influence of the Reduction of Deepwater Formation on Ocean Heat Uptake and Heat Budgets in the Global Climate System. *Geophysical Research Letters*, **49 (3)**, e2021GL095 179, https://doi.org/10.1029/2021GL095179.

Swart, N. C., and Coauthors, 2023: The Southern Ocean Freshwater Input from Antarctica (SOFIA) Initiative: scientific objectives and experimental design. *Geoscientific Model Development*, **16 (24)**, 7289–7309, https://doi.org/10.5194/gmd-16-7289-2023.

Talley, L. D., 2013: Closure of the global overturning circulation through the Indian, Pacific, and southern oceans. *Oceanography*, **26 (1)**, 80–97, https://doi.org/10.5670/OCEANOG.2013.07.

Taylor, K. E., R. J. Stouffer, and G. A. Meehl, 2012: An Overview of CMIP5 and the Experiment Design. *Bulletin of the American Meteorological Society*, **93 (4)**, 485–498, https://doi.org/10.1175/BAMS-D-11-00094.1.

Thompson, A. F., A. L. Stewart, and T. Bischoff, 2016: A Multibasin Residual-Mean Model for the Global Overturning Circulation. *Journal of Physical Oceanography*, **46 (9)**, 2583–2604, https://doi.org/10.1175/JPO-D-15-0204.1.

Todd, A., and Coauthors, 2020: Ocean-Only FAFMIP: Understanding Regional Patterns of Ocean Heat Content and Dynamic Sea Level Change. *Journal of Advances in Modeling Earth Systems*, **12 (8)**, e2019MS002 027, https://doi.org/10.1029/2019MS002027.

Weiffenbach, J. E., and Coauthors, 2024: Highly stratified mid-Pliocene Southern Ocean in PlioMIP2. *Climate of the Past*, **20 (4)**, 1067–1086, https://doi.org/10.5194/cp-20-1067-2024.

Wickramage, C., A. Köhl, J. Jungclaus, and D. Stammer, 2023: Sensitivity of MPI-ESM Sea Level Projections to Its Ocean Spatial Resolution. *Journal of Climate*, **36 (6)**, 1957–1980, https://doi.org/10.1175/JCLI-D-22-0418.1.

Winton, M., W. G. Anderson, T. L. Delworth, S. M. Griffies, W. J. Hurlin, and A. Rosati, 2014: Has coarse ocean resolution biased simulations of transient climate sensitivity? *Geophysical Research Letters*, **41 (23)**, 8522–8529, https://doi.org/10.1002/2014GL061523.

Zanna, L., J. M. Brankart, M. Huber, S. Leroux, T. Penduff, and P. D. Williams, 2019: Uncertainty and scale interactions in ocean ensembles: From seasonal forecasts to multidecadal climate predictions. *Quarterly Journal of the Royal Meteorological Society*, **145 (S1)**, 160–175, https://doi.org/10.1002/QJ.3397.

Zika, J. D., N. Skliris, A. T. Blaker, R. Marsh, A. J. G. Nurser, and S. A. Joser, 2018: Improved estimates of water cycle change from ocean salinity: the key role of ocean warming. *Environmental Research Letters*, **13 (7)**, 074 036, https://doi.org/10.1088/1748-9326/aace42.